AIMS Mathematics, 11(1): 1412–1448.
DOI: 10.3934/math.2026060
Received: 27 October 2025
Revised: 22 December 2025
Accepted: 05 January 2026
Published: 16 January 2026

http://www.aimspress.com/journal/Math

*Research article*

# Stability and bifurcation analysis of a fractional-order prey–predator model with ratio-dependent functional response

**Ibrahim Alraddadi[1], Ramesh Perumal[2], Rizwan Ahmed[3], Jawad Khan[4,*] and Youngmoon Lee[5,6,*]**

[1] Department of Mathematics, Faculty of Science, Islamic University of Madinah, Madinah, Saudi Arabia

[2] Department of Mathematics, Madanapalle Institute of Technology & Science (MITS), Deemed to be University, Madanapalle, Andhra Pradesh, India

[3] Department of Mathematics, Air University Multan Campus, Multan 60001, Pakistan

[4] School of Computing, Gachon University, Seongnam 13120, Republic of Korea

[5] Department of Robotics, Hanyang University, Ansan 15588, Republic of Korea

[6] Department of Applied AI, Hanyang University, Ansan 15588, Republic of Korea

* **Correspondence:** Email: jkhanbk1@gachon.ac.kr, youngmoonlee@hanyang.ac.kr.

**Abstract:** This paper explores the dynamics of a fractional prey–predator system with a ratio-dependent functional response with memory and hereditary effects in predator–prey interactions. The model is developed by the Caputo fractional derivative, and the existence, uniqueness, positivity, and boundedness of solutions are proven to satisfy biological reality. Stability conditions for local and global stability of both predator-free and coexistence equilibria are proven through linearization and Lyapunov function techniques. The fractional order is used as a bifurcation parameter, and the appearance of Hopf bifurcations is analytically explained with demonstration of the influence of memory on oscillations. To examine discrete-time dynamics, the piecewise constant argument is used to derive a discrete counterpart of the fractional model. The discrete model indicates a wide range of rich complex oscillatory phenomena, including period-doubling and Neimark–Sacker bifurcations, leading to periodic, quasiperiodic, and chaotic oscillations. Numerical computations, including bifurcation diagrams, phase portraits, and Lyapunov exponents, verify the analytical results and describe the routes of transition to chaos. A comparative analysis to compare integer- and fractional-order cases indicates that memory effects enhance dynamical richness and sensitivity to parameters. The study provides a unified framework relating continuous fractional dynamics and their discrete implementations and provides additional insight into how memory and discretization interact to modify stability and bifurcation in ecological models.

**Keywords:** fractional-order; prey–predator model; stability; bifurcation; chaos
**Mathematics Subject Classification:** 39A28, 39A30

## 1. Introduction

predator–prey interactions have long served as a fundamental framework in mathematical biology, capturing essential aspects of ecological dynamics between two species, one serving as a resource (prey) and the other as a consumer (predator). Classical models like the Lotka–Volterra system [1, 2] and its many variants rely on integer-order derivatives, implicitly assuming that the population rate of change relies exclusively on the current state. This is usually a simplification, ignoring memory and hereditary effects characteristic of most real-life biological systems.

To introduce memory-dependent dynamics, fractional differential equations have proved to be an extremely effective generalization of traditional models. By introducing derivatives of non-integer order, fractional-order models can effectively capture long-term interactions, delayed responses, and internal feedback mechanisms more accurately than their integer-order counterparts. In this context, fractional-order prey–predator models have gained increasing attention for their ability to reflect more realistic and complex ecological behaviors, including oscillations, extinction, and coexistence.

Several studies have demonstrated the importance of fractional derivatives in capturing the complex dynamics of prey–predator interactions more realistically. Javidi and Nyamoradi [3] investigated a fractional prey–predator model with harvesting and investigated its local and global stability properties, supported by numerical examples. Li et al. [4] examined a fractional prey–predator system with refuge, proving the existence, uniqueness, and boundedness of solutions, and obtained sufficient conditions for global asymptotic stability of equilibria. Elettreby et al. [5] analyzed a two-prey, one-predator fractional-order model, showing that certain equilibria that are centers in the integer-order case become asymptotically stable under fractional dynamics. In another work, Li et al. [6] incorporated prey refuge and feedback control into a fractional-order model and demonstrated how these mechanisms could regulate population levels effectively, with stability analyzed via characteristic equations. Sarkar and Mondal [7] explored a fractional prey–predator model with combined harvesting, establishing conditions for stability and Hopf bifurcation by treating the fractional-order as a bifurcation parameter, and emphasized the ecological implications of combined versus selective harvesting strategies. It is also worth noting that time delays arising from gestation, maturation, or response lags have been widely studied in predator–prey systems due to their significant impact on stability and oscillatory behavior [8–11].

Despite their advantages in modeling continuous-time processes, real-world data are often collected at discrete time intervals, necessitating the study of corresponding discrete-time systems. In addition, discretization may create new dynamical properties not shared with the continuous model, including period-doubling (PD), Neimark–Sacker (NS) bifurcations, and chaotic behavior. Of multiple discretization techniques, the piecewise constant argument method [12–15] offers a mathematically acceptable and biologically relevant method for discretizing continuous models into discrete-time counterparts while preserving essential dynamical characteristics.

In this paper, we initially present and study a fractional prey–predator model in terms of the Caputo

derivative. We study the existence and stability of biologically meaningful equilibria and examine the local dynamics of the continuous system. We then use the piecewise constant argument technique to get a discrete-time counterpart of the model. The resulting discrete system is subsequently analyzed with respect to its stability and bifurcations, showing that the discrete-time model exhibits significantly more complex dynamics compared to the continuous model. Surprisingly, the discretization provokes bifurcations and potential paths towards chaos, suggesting the delicate interaction between memory effects and discrete-time evolution in ecological systems.

Although the continuous-time fractional-order model and its discrete-time counterpart represent two distinct dynamical systems, they are studied simultaneously in this work for complementary reasons. The continuous fractional model is biologically motivated and captures memory and hereditary effects inherent in predator–prey interactions, allowing rigorous analysis of existence, boundedness, and stability. In contrast, the discrete model arises naturally when population processes are observed at discrete time intervals or when numerical implementation is required. Studying both formulations enables us to investigate how memory effects interact with discretization and to understand how qualitative dynamics may change when continuous ecological processes are represented in discrete time.

Our research fills the gap between continuous fractional dynamics and their discrete counterparts, offering qualitative insights into prey–predator systems under the effects of memory and discrete-time interactions. The theoretical results are supported with numerical examples, illustrating the diverse range of dynamical behaviors that can arise through fractional modeling and discretization. The main contributions of this paper are:

- A Caputo fractional prey–predator model is proposed, featuring a ratio-dependent functional response to capture more realistic interaction dynamics.
- The existence and uniqueness of solutions are established for the fractional model and show positivity and uniform boundedness of biologically relevant solutions.
- We derive local stability conditions for boundary and interior equilibria in the fractional model and provide sufficient conditions for global stability using appropriate Lyapunov functions.
- The Hopf bifurcation of the fractional model is examined with the fractional order taken as the bifurcation parameter.
- By applying the piecewise constant argument technique, the fractional system is transformed into its discrete counterpart; we derive the discrete map, classify the fixed points, and identify the parameter intervals associated with PD and NS bifurcations.
- We validate analytical findings with numerical simulations (time series, phase portraits, bifurcation diagrams, and maximum Lyapunov exponent computations) and provide practical guidance on parameter regimes that produce complex behavior (periodic/chaotic) in the discrete map.

We emphasize here that the model studied in this manuscript is mainly theoretical and is not calibrated by using any specific empirical data set. The formulation relies on well-established ecological assumptions such as ratio-dependent predation and memory effects modeled via fractional-order derivatives, which have been used in a wide sense in the literature to model realistic predator–prey interactions. The main goal of the present study is thus to understand the nature of qualitative

dynamical behavior induced by memory and discretization, such as stability, bifurcations, and chaos, rather than to give any data-driven prediction for a particular ecosystem. Nevertheless, the modeling framework is general enough and can be fitted with empirical data in future studies once appropriate ecological observations are available.

The rest of the manuscript is structured as follows. Section 2 presents the model formulation of the fractional prey–predator model with ratio-dependent functional response. Section 3 offers some mathematical preliminaries and basic results of fractional calculus. The existence and uniqueness of solutions are established in Section 4, and an analysis of positivity and boundedness of biologically meaningful solutions is provided in Section 5. Section 6 deals with the equilibrium points and analyzes their local stability, whereas Section 7 addresses global stability with appropriate Lyapunov functions. The emergence of Hopf bifurcation with change in fractional order is analyzed in Section 8, and corresponding numerical examples supporting the analytical findings are given in Section 9. Discretization of the fractional model by using the piecewise constant argument technique is presented in Section 10, and Sections 11–13 are concerned with the stability classification, bifurcation study, and numerical investigation of the discrete system. The conclusion of the study is given in Section 14.

## 2. Model formulation

Consider a prey–predator system incorporating a ratio-dependent functional response, which can be expressed as

$$\begin{cases} \frac{\mathrm{d}u}{\mathrm{d}t} = pu\left(1 - \frac{u}{q}\right) - \frac{ruv}{sv+u}, \\ \frac{\mathrm{d}v}{\mathrm{d}t} = v\left(\frac{r_1 u}{sv+u} - d\right), \end{cases} \tag{2.1}$$

where $u(t)$ and $v(t)$ represent the population densities of prey and predator, respectively, at time $t \geq 0$. $p$ represents the rate of growth of prey, and $q$ is the environmental carrying capacity of prey. $r$ is the parameter that represents the predation rate, or fraction of prey caught per predator per unit time, and $s$ is the handling time, that is the average time taken by a predator to catch and digest one prey. The constant $r_1$ represents the conversion efficiency, and $d$ is the natural death rate of the predator. The term $\frac{ru}{sv+u}$ is a Michaelis–Menten-type ratio-dependent functional response, which reflects that the per capita predation rate relies on the prey-to-predator ratio rather than on the prey density alone. Such a formulation is biologically realistic when predator interference or limited searching ability is present.

The ratio-dependent functional response is used biologically to represent predator interference and competition effects commonly observed in real ecosystems. This formulation, as compared with the classical Holling Type I functional response based on prey density alone and thus increasing linearly without saturation, describes the premise of decreased efficiency due to high predator-to-prey densities. This situation arises naturally in predators that compete for limited prey, experience mutual interference, or have restricted searching and handling capacities. Such effects are particularly relevant in ecosystems where predators interact actively with one another or where there are significant fluctuations in prey availability. Thus, the ratio-dependent functional response has, in many biological contexts, an ecologically more realistic description than that of the Holling Type I response. Mathematically, a ratio-dependent functional response increases nonlinearity due to rational terms involving both prey and predator populations, unlike the simpler polynomial form of the Holling Type I response. This adds analytical challenges, particularly in proving boundedness and stability, but these can be addressed under realistic biological assumptions like population positivity. The ratio-dependent

structure also supports the construction of Lyapunov functions and offers a more balanced predator–prey model. As shown later, the system still allows for positive invariant regions and rigorous local and global stability results despite the added complexity.

To minimize the number of parameters and simplify the analysis, we introduce the following nondimensional variables and parameters:

$$x = \frac{u}{q},\ y = \frac{sv}{q},\ t = pt,\ a = \frac{r}{sp},\ b = \frac{r_1}{p},\ c = \frac{d}{r_1}.$$

Substituting these transformations into (2.1) yields the nondimensional form

$$\begin{cases} \frac{\mathrm{d}x}{\mathrm{d}t} = x(1-x) - \frac{axy}{x+y}, \\ \frac{\mathrm{d}y}{\mathrm{d}t} = by\left(\frac{x}{x+y} - c\right). \end{cases} \tag{2.2}$$

In order to account for memory and hereditary characteristics within population dynamics, we generalize the integer-order system to a fractional form by substituting the standard time derivative with the Caputo fractional derivative of order $0 < \sigma \leq 1$. The resulting fractional-order prey–predator model is expressed as

$$\begin{cases} {}^{C}\mathrm{D}^{\sigma}x = x(1-x) - \frac{axy}{x+y}, \\ {}^{C}\mathrm{D}^{\sigma}y = by\left(\frac{x}{x+y} - c\right), \end{cases} \tag{2.3}$$

where ${}^{C}\mathrm{D}_{t}^{\sigma}$ denotes the Caputo fractional derivative. Here, $\sigma$ is the fractional order that controls the strength of memory in the system. For $\sigma = 1$, (2.3) reduces to the classical integer-order model (2.2).

From a biological perspective, the fractional order $\sigma$ represents memory and hereditary effects in predator–prey interactions. In classical integer-order models, the rate of change of populations depends only on their current state, whereas fractional-order models allow past population levels to influence the present dynamics. This feature is particularly relevant in ecological systems, where biological processes such as predator learning, delayed responses to environmental changes, gestation periods, and the accumulation of stress effects play a significant role. Smaller values of $\sigma$ correspond to stronger memory effects, which tend to damp population oscillations and enhance stability, while $\sigma = 1$ recovers the classical memoryless model. Therefore, the fractional order $\sigma$ serves as a biologically meaningful parameter that controls the strength of memory in the system.

## 3. Preliminaries

In this section, we recall some basic definitions and useful results from the theory of fractional calculus that will be used throughout this paper.

**Definition 3.1** ([16]). *The Caputo fractional derivative of order $\sigma$ for a function $f \in C^n([t_0, \infty), \mathbb{R})$ is*

$${}^{C}\mathrm{D}_{t_0}^{\sigma} f(t) = \frac{1}{\Gamma(n-\sigma)} \int_{t_0}^{t} (t-\tau)^{n-\sigma-1} f^{(n)}(\tau) d\tau, \tag{3.1}$$

*where $\Gamma(n)$ is the standard Gamma function, $t \geq t_0$ and $n \in \mathbb{N}$ satisfying $n-1 < \sigma < n$. Particularly, when $0 < \sigma < 1$, then*

$${}^{C}\mathrm{D}_{t_0}^{\sigma} f(t) = \frac{1}{\Gamma(1-\sigma)} \int_{t_0}^{t} (t-\tau)^{-\sigma} f'(\tau) d\tau. \tag{3.2}$$

The following lemmas describe some important properties of fractional derivatives that are frequently employed in qualitative analysis, such as monotonicity and boundedness.

**Lemma 3.2** ([17]). *Let $0 < \sigma \leq 1$. Assume $f \in C[a, b]$ and its Caputo fractional derivative ${}^{C}\mathrm{D}^{\sigma} f(t) \in C[a, b]$.*

*(1) If ${}^{C}\mathrm{D}^{\sigma} f(t) \geq 0\ \forall t \in (a, b)$, then $f$ is nondecreasing on $[a, b]$.*

*(2) If ${}^{C}\mathrm{D}^{\sigma} f(t) \leq 0\ \forall t \in (a, b)$, then $f$ is nonincreasing on $[a, b]$.*

**Lemma 3.3** ([4]). *Let $u(t)$ be a continuous function on $[t_0, \infty)$ satisfying*

$$ {}^{C}\mathrm{D}^{\sigma} u(t) \leq -\xi u(t) + \rho, \quad u(t_0) = u_{t_0}, $$

*where $0 < \sigma \leq 1$ and $(\xi, \rho) \in \mathbb{R}^2$, $\xi \neq 0$, and $t_0 \geq 0$ denotes the starting time. Then, the function $u(t)$ satisfies the inequality*

$$ u(t) \leq \left( u_{t_0} - \frac{\rho}{\xi} \right) E_{\sigma}[-\xi (t - t_0)^{\sigma}] + \frac{\rho}{\xi}, $$

*where $E_{\sigma}(\cdot)$ denotes the Mittag-Leffler function.*

The following result provides the linear stability criterion for equilibrium points of a fractional dynamical system.

**Theorem 3.4** ([18]). *Consider the fractional-order system*

$$ {}^{C}\mathrm{D}^{\sigma}_{t_0} z(t) = f(z), \quad z(0) = z_0, $$

*where $0 < \sigma \leq 1$, $z \in \mathbb{R}^n$, and $f : \mathbb{R}^n \to \mathbb{R}^n$. The equilibrium points are obtained by solving $f(z) = 0$. Let $J = \frac{\partial f}{\partial z}$ be the Jacobean matrix determined at an equilibrium point. Then, the equilibrium is locally asymptotically stable (LAS) if all eigenvalues $\omega_i$ of $J$ fulfill*

$$ |\arg(\omega_i)| > \frac{\sigma \pi}{2}, \quad i = 1, 2, \ldots, n. $$

## 4. Existence and uniqueness

In this section, we establish the existence and uniqueness of solutions for the fractional prey–predator model (2.3). To do so, we first recall a standard lemma concerning the local existence and uniqueness of solutions for Caputo fractional differential equations.

**Lemma 4.1** ([19]). *Consider the fractional-order system*

$$ {}^{C}\mathrm{D}^{\sigma}_{t_0} z(t) = f(t, z), \quad t > t_0 \tag{4.1} $$

*with the initial value $z(t_0) = z_{t_0}$, where $\sigma \in (0, 1]$. Assume that $f : [t_0, \infty) \times \Omega \to \mathbb{R}^n$ with $\Omega \subset \mathbb{R}^n$, fulfills the locally Lipschitz condition w.r.t. $z$. Then, (4.1) admits a unique solution on $[t_0, \infty) \times \Omega$.*

**Theorem 4.2.** *For every $(x_0, y_0) \in \Omega$, there exists a unique solution $X = (x, y) \in \Omega$ of (2.3), where $\Omega = \{ (x, y) : \max\{|x|, |y|\} \leq M \}$.*

*Proof.* Consider the fractional prey–predator system defined by

$$H_1(x,y) = x(1-x) - \frac{axy}{x+y},$$
$$H_2(x,y) = by\left(\frac{x}{x+y} - c\right).$$

Because $x, y > 0$ are bounded above by $M$, we can therefore select $\xi > 0$ s.t. $|x+y| \geq \xi > 0$.
Let $X = (x,y)^T$, $\widehat{\mathtt{X}} = (\widehat{\mathtt{x}}, \widehat{\mathtt{y}})^T$. Define

$$\begin{aligned}
\|H(X) - H(\widehat{\mathtt{X}})\| &= |H_1(x,y) - H_1(\widehat{\mathtt{x}},\widehat{\mathtt{y}})| + |H_2(x,y) - H_2(\widehat{\mathtt{x}},\widehat{\mathtt{y}})| \\
&= \left|x(1-x) - \widehat{\mathtt{x}}(1-\widehat{\mathtt{x}}) - a\left(\frac{xy}{x+y} - \frac{\widehat{\mathtt{xy}}}{\widehat{\mathtt{x}}+\widehat{\mathtt{y}}}\right)\right| + b\left|y\left(\frac{x}{x+y} - c\right) - \widehat{\mathtt{y}}\left(\frac{\widehat{\mathtt{x}}}{\widehat{\mathtt{x}}+\widehat{\mathtt{y}}} - c\right)\right| \\
&\leq |x-\widehat{\mathtt{x}}| + |x^2 - \widehat{\mathtt{x}}^2| + a\left|\frac{xy}{x+y} - \frac{\widehat{\mathtt{xy}}}{\widehat{\mathtt{x}}+\widehat{\mathtt{y}}}\right| + bc|y-\widehat{\mathtt{y}}| + b\left|\frac{xy}{x+y} - \frac{\widehat{\mathtt{xy}}}{\widehat{\mathtt{x}}+\widehat{\mathtt{y}}}\right| \\
&\leq |x-\widehat{\mathtt{x}}| + |x+\widehat{\mathtt{x}}||x-\widehat{\mathtt{x}}| + a\left(\frac{x\widehat{\mathtt{x}}|y-\widehat{\mathtt{y}}| + y\widehat{\mathtt{y}}|x-\widehat{\mathtt{x}}|}{(x+y)(\widehat{\mathtt{x}}+\widehat{\mathtt{y}})}\right) + bc|y-\widehat{\mathtt{y}}| + b\left(\frac{x\widehat{\mathtt{x}}|y-\widehat{\mathtt{y}}| + y\widehat{\mathtt{y}}|x-\widehat{\mathtt{x}}|}{(x+y)(\widehat{\mathtt{x}}+\widehat{\mathtt{y}})}\right) \\
&\leq \left(1 + 2M + \frac{(a+b)M^2}{\xi^2}\right)|x-\widehat{\mathtt{x}}| + \left(bc + \frac{(a+b)M^2}{\xi^2}\right)|y-\widehat{\mathtt{y}}| \\
&\leq L\|X - \widehat{\mathtt{X}}\|,
\end{aligned}$$

where

$$L = \max\left\{1 + 2M + \frac{(a+b)M^2}{\xi^2}, bc + \frac{(a+b)M^2}{\xi^2}\right\}.$$

Therefore, $H(X)$ fulfills the Lipschitz condition; it follows from Lemma 4.1 that there exists a unique solution $X(t)$ of (2.3). □

Theorem 4.2 ensures that the fractional prey–predator model (2.3) is well-posed in the sense of existence and uniqueness of solutions.

## 5. Nonnegativity and boundedness

Considering the biological relevance of the model, we focus only on solutions that remain nonnegative and bounded. The next theorem guarantees the nonnegativity and boundedness of the solutions of (2.3). Define

$$\Omega_+ = \{(x,y) \in \Omega : x \in \mathbb{R}_+,\ y \in \mathbb{R}_+\}.$$

**Theorem 5.1.** *Every solution of* (2.3) *that begins in* $\Omega_+$ *remains nonnegative and uniformly bounded* $\forall t \geq 0$.

*Proof.* We first show that the solutions $x(t)$ originating in $\Omega_+$ remain nonnegative. Assume on the contrary that this is not the case. Then, there exists $t_1 > 0$ s.t.

$$x(t) > 0, \quad 0 \leq t < t_1, \quad x(t_1) = 0, \quad x(t_1^+) < 0.$$

Then, from (2.3), we obtain

$$^{C}\mathrm{D}^{\sigma}x(t)\Big|_{t=t_1} = 0.$$

Using Lemma 3.2, we obtain $x(t_1^+) = 0$. This contradicts the assumption that $x(t_1^+) < 0$. Hence, $x(t) \geq 0$ for all $t \geq 0$. By applying similar reasoning, it follows that $y(t) \geq 0$ for all $t \geq 0$.

We now demonstrate that all solutions of (2.3) originating in $\mathbb{R}_2^+$ are uniformly bounded. Define $V(t) = x(t) + \frac{a}{b}y(t)$, then

$$^{C}\mathrm{D}^{\sigma}V(t) + bcV(t) = -x^2 + bcx = -\Big(x - \frac{1+bc}{2}\Big)^2 + \Big(\frac{1+bc}{2}\Big)^2 \leq \Big(\frac{1+bc}{2}\Big)^2.$$

Using Lemma 3.3, we have

$$V(t) \leq \Big(V(t_0) - \frac{(1+bc)^2}{4bc}\Big) + E_{\sigma}[-bc(t-t_0)^{\sigma}] + \frac{(1+bc)^2}{4bc} \longrightarrow \frac{(1+bc)^2}{4bc}, t \to \infty.$$

Therefore, all the solutions of (2.3) starting in $\Omega_+$ are confined to the region $\mathbb{S}$, where

$$\mathbb{S} = \Big\{(x,y) \in \mathbb{R}_+^2 : x + \frac{a}{b}y \leq \frac{(1+bc)^2}{4bc} + \epsilon, \epsilon > 0\Big\}.$$

This completes the proof. □

## 6. Equilibrium points and local stability

In this section, we find all equilibrium points of (2.3) and analyze their local stability properties by applying the linearization method for fractional-order systems.

The equilibrium points of (2.3) are obtained by solving the following equations:

$$\begin{cases} x(1-x) - \frac{axy}{x+y} = 0, \\ by\Big(\frac{x}{x+y} - c\Big) = 0. \end{cases} \tag{6.1}$$

There are two equilibrium points:

(i) The boundary equilibrium point is $E_1 = (1, 0)$.

(ii) The positive equilibrium point $E^* = \Big(1 - a(1-c), \frac{[1-a(1-c)](1-c)}{c}\Big)$. $E^*$ exists only if $\frac{a-1}{a} < c < 1$.

The Jacobian matrix $J$ of (2.3) is

$$J(x,y) = \begin{bmatrix} 1 - \frac{ay}{x+y} + x\Big(\frac{ay}{(x+y)^2} - 2\Big) & -\frac{ax^2}{(x+y)^2} \\ \frac{by^2}{(x+y)^2} & b\Big(\frac{x^2}{(x+y)^2} - c\Big) \end{bmatrix}. \tag{6.2}$$

**Proposition 6.1.** *The equilibrium point $E_1 = (1, 0)$ is*

*(1) LAS if $c > 1$,*

*(2) a saddle point if $c < 1$.*

*Proof.* We obtain

$$J(E_1) = \begin{bmatrix} -1 & -a \\ 0 & b(1-c) \end{bmatrix}. \tag{6.3}$$

The eigenvalues of $J(E_1)$ are $\omega_1 = -1$ and $\omega_2 = b(1-c)$. If $c > 1$, then $\omega_2 < 0$. Consequently, we get $|arg(\omega_{1,2})| = \pi > \frac{\sigma\pi}{2}$. If $c < 1$, then $\omega_2 > 0$. Consequently, we get $|arg(\omega_1)| = \pi$ but $|arg(\omega_2)| = 0$. □

Next, we investigate the positive stationary point $E^*$. The Jacobian matrix is

$$J(E^*) = \begin{bmatrix} -1 + a - ac^2 & -ac^2 \\ b(-1+c)^2 & b(-1+c)c \end{bmatrix}.$$

The corresponding characteristic polynomial is

$$\omega^2 - T\omega + D = 0, \tag{6.4}$$

where $T = -1 + a + b(-1+c)c - ac^2$ and $D = -b(1 + a(-1+c))(-1+c)c$. The eigenvalues of $J(E^*)$ are $\omega_{1,2} = \frac{T \pm \sqrt{T^2 - 4D}}{2}$. Therefore, we get the next result:

**Theorem 6.2.** *For the fractional model* (2.3)*, the interior equilibrium point $E^*$ is LAS if either of the subsequent conditions is satisfied:*

*(1) $T < 0$ and $T^2 - 4D \geq 0$,*

*(2) $T^2 - 4D < 0$ and $\frac{\sqrt{|T^2 - 4D|}}{T} > \tan(\frac{\sigma\pi}{2})$.*

*Proof.* (1) Because $T < 0$ and $T^2 - 4D \geq 0$, therefore $\omega_{1,2} < 0$ and $arg(\omega_{1,2}) = \pi > \frac{\sigma\pi}{2}$. Therefore, $E^*$ is LAS.

(2) Because $T^2 - 4D < 0$, therefore $J(E^*)$ has complex eigenvalues $\omega$ and $\bar{\omega}$. We have that

$$|\frac{\omega - \bar{\omega}}{\omega + \bar{\omega}}| = |\frac{Im(\omega)}{Re(\omega)}| = arg(\omega) = \frac{\sqrt{|T^2 - 4D|}}{T}.$$

Therefore, $E^*$ is LAS if $\frac{\sqrt{|T^2 - 4D|}}{T} > \tan(\frac{\sigma\pi}{2})$.

□

## 7. Global stability analysis

In this section, we analyze the global stability of the equilibrium points of the fractional model (2.3). To establish the results, we construct appropriate Lyapunov functions and utilize a relevant fractional inequality.

**Lemma 7.1** ([20])**.** *Consider a continuous and differentiable function $z(t) \in \mathbb{R}_+$. Then, for all $t \geq t_0$, we obtain*

$${}^{C}\mathrm{D}^{\sigma}_{t_0}\Big[z(t) - z^* - z^* \ln(\frac{z(t)}{z^*})\Big] \leq \Big(1 - \frac{z^*}{z(t)}\Big)\, {}^{C}\mathrm{D}^{\sigma}_{t_0} z(t), z^* \in \mathbb{R}_+, \forall \sigma \in (0,1).$$

The above inequality is a fractional-order analogue of the classical derivative property used in Lyapunov analysis and will be applied to establish global asymptotic stability.

**Theorem 7.2.** *If $c \geq 1$, the predator-free equilibrium point $E_1 = (1, 0)$ of (2.3) is globally asymptotically stable.*

*Proof.* Define

$$V(x, y) = x - 1 - \ln(x) + \frac{a}{b}y.$$

Evaluating the $\sigma$-order derivative of $V(x, y)$ along the solution trajectories of system (2.3) and invoking Lemma 7.1, gives

$$\begin{aligned}
{}^{C}\mathrm{D}^{\sigma}_{t_0}V &\leq \Big(\frac{x-1}{x}\Big)\,{}^{C}\mathrm{D}^{\sigma}_{t_0}x(t) + \frac{a}{b}\,{}^{C}\mathrm{D}^{\sigma}_{t_0}y(t)\\
&= (x-1)\Big(-(x-1) - \frac{ay}{x+y}\Big) + ay\Big(\frac{x}{x+y} - c\Big)\\
&= -(x-1)^2 + \Big(\frac{1}{x+y} - c\Big)ay\\
&\leq -(x-1)^2 + (1-c)ay.
\end{aligned}$$

Thus, for $c \geq 1$, we have ${}^{C}\mathrm{D}^{\sigma}_{t_0}V \leq 0$ for all $(x, y) \in \mathbb{R}^2_+$. Moreover, ${}^{C}\mathrm{D}^{\sigma}_{t_0}V = 0$ at $E_1$. It follows that $E_1 = (1, 0)$ attains global asymptotic stability whenever $c \geq 1$. □

**Theorem 7.3.** *The equilibrium point $E^* = (\widehat{\mathtt{x}}, \widehat{\mathtt{y}})$ of (2.3) is globally asymptotically stable in $\Big\{(x, y) : \frac{y}{\widehat{\mathtt{y}}} > \frac{x}{\widehat{\mathtt{x}}} > 1\Big\}$.*

*Proof.* We introduce the Lyapunov function

$$V(x, y) = \left(x - \widehat{\mathtt{x}} - \widehat{\mathtt{x}}\ln\frac{x}{\widehat{\mathtt{x}}}\right) + \frac{a}{b}\left(y - \widehat{\mathtt{y}} - \widehat{\mathtt{y}}\ln\frac{y}{\widehat{\mathtt{y}}}\right).$$

Evaluating the $\sigma$-order derivative of $V(x, y)$ along the solution trajectories of system (2.3) and invoking Lemma 7.1, gives

$$\begin{aligned}
{}^{C}\mathrm{D}^{\sigma}_{t_0}V &\leq \Big(\frac{x-\widehat{\mathtt{x}}}{x}\Big)\,{}^{C}\mathrm{D}^{\sigma}_{t_0}x(t) + \frac{a}{b}\Big(\frac{y-\widehat{\mathtt{y}}}{y}\Big)\,{}^{C}\mathrm{D}^{\sigma}_{t_0}y(t)\\
&= (x-\widehat{\mathtt{x}})\Big(1 - x - \frac{ay}{x+y}\Big) + a(y-\widehat{\mathtt{y}})\Big(\frac{x}{x+y} - c\Big)\\
&= (x-\widehat{\mathtt{x}})\Big(1 - x - \frac{ay}{x+y} - (1-\widehat{\mathtt{x}}) + \frac{a\widehat{\mathtt{y}}}{\widehat{\mathtt{x}}+\widehat{\mathtt{y}}}\Big) + a(y-\widehat{\mathtt{y}})\Big(\frac{x}{x+y} - \frac{\widehat{\mathtt{x}}}{\widehat{\mathtt{x}}+\widehat{\mathtt{y}}}\Big)\\
&= -(x-\widehat{\mathtt{x}})^2 + a(x-\widehat{\mathtt{x}})\Big(\frac{\widehat{\mathtt{y}}}{\widehat{\mathtt{x}}+\widehat{\mathtt{y}}} - \frac{y}{x+y}\Big) + a(y-\widehat{\mathtt{y}})\Big(\frac{x}{x+y} - \frac{\widehat{\mathtt{x}}}{\widehat{\mathtt{x}}+\widehat{\mathtt{y}}}\Big)\\
&= -(x-\widehat{\mathtt{x}})^2 + \frac{a(x\widehat{\mathtt{y}} - \widehat{\mathtt{x}}y)}{(x+y)(\widehat{\mathtt{x}}+\widehat{\mathtt{y}})}\Big((x-\widehat{\mathtt{x}}) + (y-\widehat{\mathtt{y}})\Big).
\end{aligned}$$

Hence, ${}^{C}\mathrm{D}^{\sigma}_{t_0}V \leq 0$ in the set $\Big\{(x, y) : \frac{y}{\widehat{\mathtt{y}}} > \frac{x}{\widehat{\mathtt{x}}} > 1\Big\}$. Moreover, ${}^{C}\mathrm{D}^{\sigma}_{t_0}V = 0$ at $E^*$. □

The above theorems confirm that both equilibria of (2.3) possess global stability under appropriate parameter conditions.

## 8. Hopf bifurcation

Hopf bifurcation occurs when two complex conjugate eigenvalues of the Jacobian cross the imaginary axis as a parameter changes, resulting in the emergence of periodic oscillations from a stable focus. In the context of fractional-order systems, this transition is influenced not only by system parameters but also by the fractional order $\sigma$, which can serve as a bifurcation parameter controlling the onset of oscillatory behavior.

**Lemma 8.1** ([21–23])**.** *Assume that the following conditions are fulfilled:*

*(1) the Jacobian matrix $J(E^*)$ of* (2.3) *has a pair of complex conjugate eigenvalues with positive real part*

*(2)* $p(\sigma_0) = \frac{\sigma_0\pi}{2} - \min_{1\le i\le 2}|arg(\omega_i)| = 0$,

*(3)* $\frac{dp(\sigma)}{d\sigma}|_{\sigma=\sigma_0} \neq 0$;

*then,* (2.3) *experiences a Hopf bifurcation at $E^*$ when the bifurcation parameter $\sigma$ crosses $\sigma_0$.*

**Theorem 8.2.** *If $T^2 - 4D < 0$ and $T > 0$, then a Hopf bifurcation of* (2.3) *will appear around $E^*$ when $\sigma$ crosses the critical value*

$$\sigma_0 = \frac{2}{\pi}\tan^{-1}\Big(\frac{\sqrt{|T^2 - 4D|}}{T}\Big).$$

*Proof.* Denote $\nu = \frac{T}{2}$ and $\phi = \frac{\sqrt{|T^2 - 4D|}}{2}$. Clearly, $\nu > 0$. Because $T^2 - 4D < 0$, the eigenvalues of $J(E^*)$ are a pair of complex conjugates $\omega_{1,2} = \nu + i\phi$. Next,

$$\begin{aligned} p(\sigma_0) &= \frac{\sigma_0\pi}{2} - \min_{1\le i\le 2}|arg(\omega_i)| \\ &= \frac{\sigma_0\pi}{2} - arg\Big(\frac{\phi}{\nu}\Big) = arg\Big(\frac{\phi}{\nu}\Big) - arg\Big(\frac{\phi}{\nu}\Big) = 0. \end{aligned}$$

Finally,

$$\frac{dp(\sigma)}{d\sigma}|_{\sigma=\sigma_0} = \frac{\pi}{2} \neq 0.$$

Using Lemma 8.1, we can infer that a Hopf bifurcation will occur at $E^*$ when $\sigma$ crosses

$$\sigma_0 = \frac{2}{\pi}\tan^{-1}\Big(\frac{\sqrt{|T^2 - 4D|}}{T}\Big).$$

The proof is completed. □

**Remark 8.3.** *The theorem above emphasizes the important role played by the fractional order $\sigma$ in determining system behavior. In contrast to the traditional integer-order scenario, where Hopf bifurcation is solely dependent upon model parameters, in the fractional-order scenario, $\sigma$ is another bifurcation parameter. A smaller $\sigma$ tends to increase system memory and damping, retarding or even eliminating oscillatory behavior.*

## 9. Numerical examples for the continuous model (2.3)

Here we present numerical examples to confirm the analytical results obtained for the fractional prey–predator model with ratio-dependent response. Numerical simulations are carried out by utilizing the Adams-type predictor-corrector method [24, 25], which is a robust and popular numerical scheme for solving fractional-order equations. Namely, we use the PECE (Predict, Evaluate, Correct, Evaluate) algorithm of the Caputo derivative with a constant step size $h = 2^{-6}$.

Our computational study examines the local and global dynamic properties of the system, that is, convergence to equilibria, oscillatory dynamics, and initial condition dependence. All simulations are run under biologically realistic parameter sets that guarantee positivity and boundedness of solutions, as established previously.

### *9.1. Transition from oscillations to stability as $\sigma$ decreases*

We set $a = 1.55, b = 0.92, c = 0.45$, with initial populations $x_0 = 0.5$, $y_0 = 0.2$. These values satisfy the conditions required for local asymptotic stability of the interior equilibrium $E^*$ as discussed in Theorem 6.2.

We simulate the system for different values of $\sigma \in \{1, 0.95, 0.90\}$ and present the corresponding phase portraits and time series in Figure 1:

- For $\sigma = 1$, the solution exhibits sustained oscillations, indicating a limit cycle about $E^*$.
- When $\sigma = 0.99$ and $\sigma = 0.98$, the amplitude of oscillations diminishes, and the system slowly converges to $E^*$, highlighting the damping effect introduced by fractional-order memory.
- Further reduction to $\sigma = 0.90$ results in faster convergence without noticeable oscillations, confirming enhanced asymptotic stability due to the fractional dynamics.

These observations illustrate how decreasing the fractional order improves stability and suppresses oscillations, even when the integer-order system may exhibit cyclic behavior.

### *9.2. Global attractivity of the interior equilibrium*

We assess the sensitivity of the system to different initial values by fixing $a = 1.55, b = 0.92, c = 0.45, \sigma = 0.95$. Four distinct initial population pairs are tested:

- $(x_0, y_0) = (0.1, 0.2)$;
- $(x_0, y_0) = (0.6, 0.2)$;
- $(x_0, y_0) = (0.4, 0.1)$;
- $(x_0, y_0) = (0.2, 0.2)$.

As depicted in Figure 2, regardless of the initial condition, the system converges to the same interior equilibrium $E^* = (0.404975, 0.384431)$. This behavior is consistent and verifies the global attractivity of the coexistence equilibrium, complementing the results of global stability proven in Theorem 7.3. It indicates the system's resilience and insensitivity to initial population oscillations.

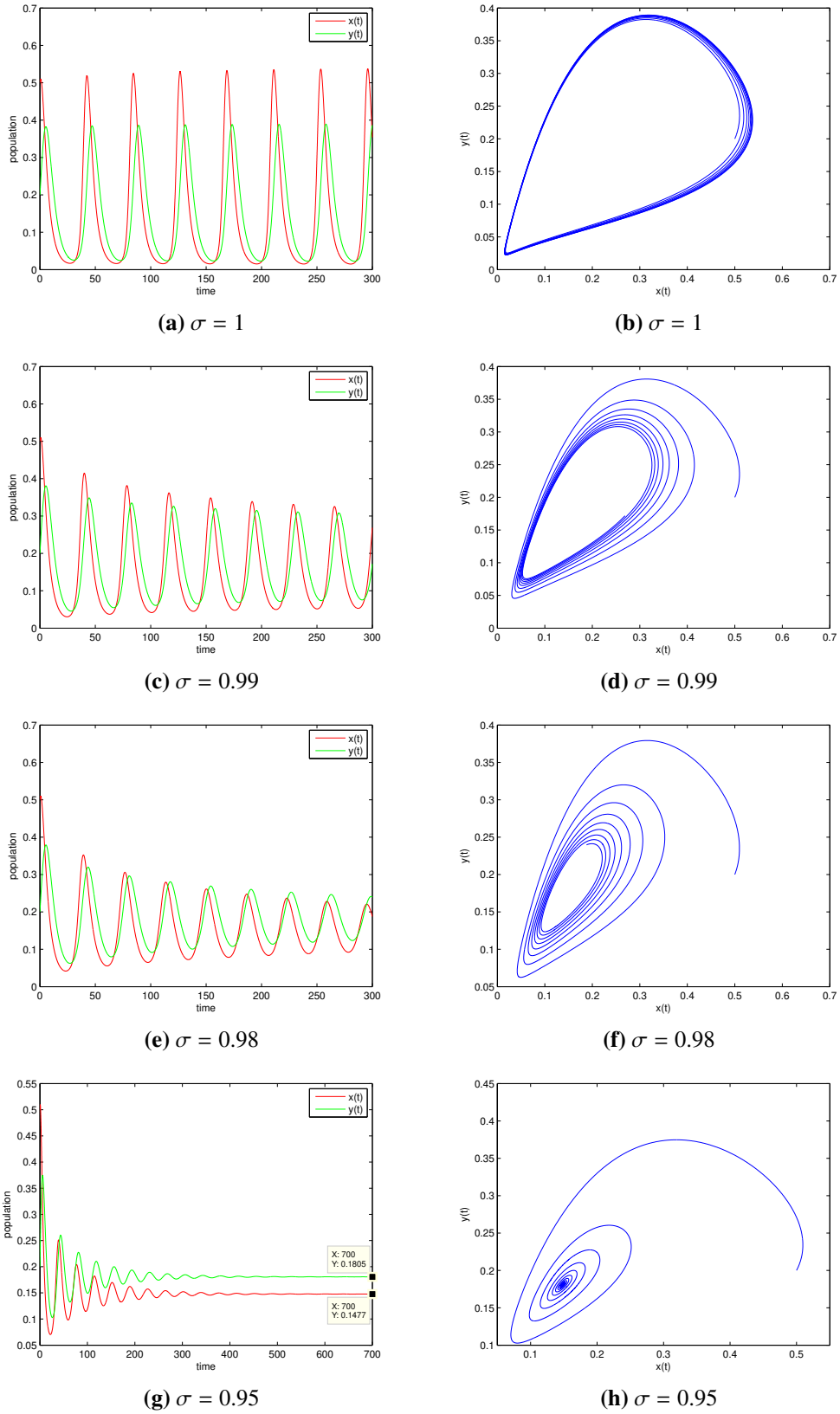


**(a)** $\sigma = 1$ **(b)** $\sigma = 1$

**(c)** $\sigma = 0.99$ **(d)** $\sigma = 0.99$

**(e)** $\sigma = 0.98$ **(f)** $\sigma = 0.98$

**(g)** $\sigma = 0.95$ **(h)** $\sigma = 0.95$

**Figure 1.** Time series and phase portraits for (2.3) with $a = 1.55, b = 0.92, c = 0.45$, and $x(0) = 0.5,\ y(0) = 0.2$, showing the effect of decreasing $\sigma$.

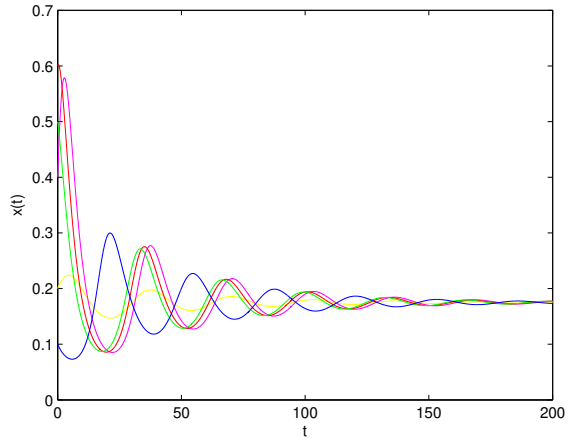


**(a)** Time series plots of $x(t)$

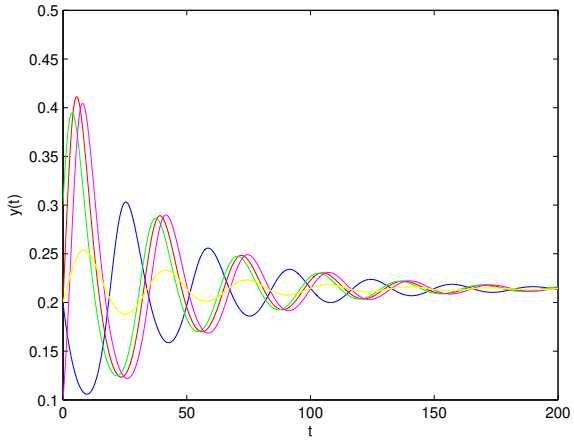


**(b)** Time series plots of $y(t)$

**Figure 2.** Time series plots for (2.3) with $a = 1.55, b = 0.92, c = 0.45, \sigma = 0.95$, and different initial values, showing convergence to $E^*$.

## 10. Discretized model

To study the discrete-time dynamics of the corresponding continuous fractional-order system (2.3), we use the piecewise constant approximation method. This method transforms the continuous system into a discrete map by approximating the state variables as constant on small subintervals of fixed duration $\theta > 0$. This kind of discretization captures the qualitative properties of the original system but permits the application of discrete dynamical tools to study stability and bifurcations. We emphasize that the discrete-time system derived via the piecewise constant argument method is not intended to be a simple numerical approximation of the continuous fractional model, but rather a mathematically consistent discrete analogue. While both models share the same equilibrium points, their dynamical behaviors may differ significantly due to the effects of discretization. In particular, discrete-time systems are known to exhibit richer dynamics, including PD cascades and NS bifurcations, even when the corresponding continuous system remains stable.

Let the initial conditions of (2.3) be $x(0) = x_0$ and $y(0) = y_0$. Then, by applying the piecewise constant approximation, the fractional model (2.3) can be written as

$$\begin{cases} {}^{C}\mathrm{D}^{\sigma}x(t) = x\Big([\frac{t}{\theta}]\theta\Big)\Big(1 - x\Big([\frac{t}{\theta}]\theta\Big)\Big) - \dfrac{ax\Big([\frac{t}{\theta}]\theta\Big)y\Big([\frac{t}{\theta}]\theta\Big)}{x\Big([\frac{t}{\theta}]\theta\Big)+y\Big([\frac{t}{\theta}]\theta\Big)}, \\ {}^{C}\mathrm{D}^{\sigma}y(t) = by\Big([\frac{t}{\theta}]\theta\Big)\left(\dfrac{x\Big([\frac{t}{\theta}]\theta\Big)}{x\Big([\frac{t}{\theta}]\theta\Big)+y\Big([\frac{t}{\theta}]\theta\Big)} - c\right). \end{cases} \tag{10.1}$$

Consider $t \in [0, \theta)$, thus $\frac{t}{\theta} \in [0, 1)$. Therefore, we obtain that

$$\begin{cases} {}^{C}\mathrm{D}^{\sigma}x_1(t) = x_0\Big(1 - x_0\Big) - \frac{ax_0y_0}{x_0+y_0}, \\ {}^{C}\mathrm{D}^{\sigma}y_1(t) = by_0\left(\frac{x_0}{x_0+y_0} - c\right). \end{cases} \tag{10.2}$$

The solution to Eq (10.2) is given by:

$$\begin{cases} x_1(t) = x_0 + \frac{t^\sigma}{\Gamma(\sigma+1)}\Big(x_0\Big(1 - x_0\Big) - \frac{ax_0y_0}{x_0+y_0}\Big), \\ y_1(t) = y_0 + \frac{t^\sigma}{\Gamma(\sigma+1)}\Big(by_0\left(\frac{x_0}{x_0+y_0} - c\right)\Big). \end{cases} \tag{10.3}$$

Next, for $t \in [\theta, 2\theta)$, and taking $\frac{t}{\theta} \in [1, 2)$, one has

$$\begin{cases} {}^C\mathrm{D}^\sigma x_2(t) = x_1\Big(1 - x_1\Big) - \frac{ax_1y_1}{x_1+y_1}, \\ {}^C\mathrm{D}^\sigma y_2(t) = by_1\left(\frac{x_1}{x_1+y_1} - c\right). \end{cases} \tag{10.4}$$

The solution to Eq (10.4) is given by:

$$\begin{cases} x_2(t) = x_1 + \frac{(t-\theta)^\sigma}{\Gamma(\sigma+1)}\Big(x_1\Big(1 - x_1\Big) - \frac{ax_1y_1}{x_1+y_1}\Big), \\ y_2(t) = y_1 + \frac{(t-\theta)^\sigma}{\Gamma(\sigma+1)}\Big(by_1\left(\frac{x_1}{x_1+y_1} - c\right)\Big). \end{cases} \tag{10.5}$$

Upon iterating the discretization proccess $n$-times, we get

$$\begin{cases} x_{n+1}(t) = x_n(n\theta) + \frac{(t-\theta)^\sigma}{\Gamma(\sigma+1)}\Big(x_n(n\theta)\Big(1 - x_n(n\theta)\Big) - \frac{ax_n(n\theta)y_n(n\theta)}{x_n(n\theta)+y_n(n\theta)}\Big), \\ y_{n+1}(t) = y_n(n\theta) + \frac{(t-\theta)^\sigma}{\Gamma(\sigma+1)}\Big(by_n(n\theta)\left(\frac{x_n(n\theta)}{x_n(n\theta)+y_n(n\theta)} - c\right)\Big), \end{cases} \tag{10.6}$$

where $t \in [n\theta, (n+1)\theta)$. For $t \to (n+1)\theta$, we obtain the following from (10.6):

$$\begin{cases} x_{n+1} = x_n + M\Big(x_n(1 - x_n) - \frac{ax_ny_n}{x_n+y_n}\Big), \\ y_{n+1} = y_n + M\Big(by_n(\frac{x_n}{x_n+y_n} - c)\Big). \end{cases} \tag{10.7}$$

Here, $M = \frac{\theta^\sigma}{\Gamma(\sigma+1)} > 0$ is the effective sampling step that embeds both the sampling rate $\theta$ and fractional-order parameter $\sigma$. The resulting discrete-time system (10.7) retains the major nonlinear interactions of the original continuous model and provides a basis for stability, bifurcations, and possible chaotic behavior to be analyzed in the discrete-time setting. It is important to note that the discrete-time model obtained in this work depends on the chosen discretization scheme. Different discretization methods may lead to discrete systems with different dynamics.

**Remark 10.1.** *The parameter $M = \frac{\theta^\sigma}{\Gamma(\sigma+1)}$ plays a crucial role in the discrete-time system* (10.7)*, as it naturally combines the sampling step size $\theta$ and the fractional order $\sigma$. From a dynamical viewpoint, $M$ governs the intensity of discrete updating and determines the extent to which past states influence the current evolution of the system. For a fixed $\sigma$, increasing the step size $\theta$ leads to a larger value of $M$, which may destabilize fixed points and give rise to PD and NS bifurcations. Conversely, when $\theta$ is fixed, decreasing the fractional order $\sigma$ reduces $M$, indicating stronger memory effects and enhanced damping in the discrete dynamics. Consequently, $M$ serves as an effective control parameter that integrates the effects of discretization intensity and memory in the discrete fractional-order predator–prey model. Although the discrete system does not explicitly preserve the nonlocal memory structure of the continuous fractional model, the memory effect is implicitly embedded through the dependence of $M$ on the fractional order $\sigma$.*

## 11. Topological classification of fixed points of the discrete model

In this section, we examine the local dynamics of (10.7) by analyzing the nature of its fixed points. The goal is to classify these equilibria according to their topological type (sink, source, saddle, or non-hyperbolic) using the eigenvalues of the Jacobian matrix.

To determine the fixed points $(x, y)$ of (10.7), we solve

$$\begin{cases} x = x + M\Big(x(1-x) - \frac{axy}{x+y}\Big), \\ y = y + M\Big(by(\frac{x}{x+y} - c)\Big). \end{cases} \tag{11.1}$$

One can see that the fixed points of (10.7) are the same as for (2.3), which are

$$E_1 = (1, 0) \text{ and } E^* = \left(1 - a(1-c), \frac{[1-a(1-c)](1-c)}{c}\right).$$

The Jacobian matrix of (10.7) at $(x, y)$ is

$$J(x, y) = \begin{bmatrix} 1 + M - \frac{aMy}{x+y} + Mx(-2 + \frac{ay}{(x+y)^2}) & -\frac{aMx^2}{(x+y)^2} \\ \frac{bMy^2}{(x+y)^2} & 1 + bM(-c + \frac{x^2}{(x+y)^2}) \end{bmatrix}. \tag{11.2}$$

Let $\omega_1$ and $\omega_2$ be the eigenvalues of $J(x, y)$. The fixed points of (10.7) can be characterized based on the modulus of these eigenvalues:

**Definition 11.1.** *A fixed point $(x, y)$ of the system is categorized as follows:*

*(1) a* sink*, if both eigenvalues $\omega_{1,2}$ satisfy $|\omega_{1,2}| < 1$,*

*(2) a* source*, if both eigenvalues satisfy $|\omega_{1,2}| > 1$,*

*(3) a* saddle*, if $\max\{|\omega_1|, |\omega_2|\} > 1$ and $\min\{|\omega_1|, |\omega_2|\} < 1$,*

*(4)* non-hyperbolic*, if at least one of the eigenvalues fulfills $|\omega_i| = 1$ for $i = 1, 2$.*

We obtain

$$J(E_1) = \begin{bmatrix} 1 - M & -aM \\ 0 & 1 + bM - bcM \end{bmatrix}. \tag{11.3}$$

The eigenvalues of $J(E_1)$ are $\omega_1 = 1 - M$ and $\omega_2 = 1 + bM - bcM$. Thus, we get the next result:

**Theorem 11.2.** *$E_1 = (1, 0)$ is*

*(1) a sink if $c > 1$, $0 < M < 2$ and $0 < b < \frac{2}{M(c-1)}$;*

*(2) a source if any one of the subsequent is met:*

*i. $M > 2$ and $0 < c < 1$,*

*ii. $M > 2$, $c > 1$ and $b > \frac{2}{M(c-1)}$;*

*(3) a saddle if one of the subsequent is fulfilled:*

*i.* $0 < M < 2$ *and* $0 < c < 1$,

*ii.* $0 < M < 2,\ c > 1$ *and* $b > \frac{2}{M(c-1)}$,

*iii.* $M > 2,\ c > 1$ *and* $0 < b < \frac{2}{M(c-1)}$;

*(4) non-hyperbolic if any of the subsequent is fulfilled:*

*i.* $M = 2$,

*ii.* $c = 1$,

*iii.* $c > 1$ *and* $b = \frac{2}{M(c-1)}$.

To categorize $E^*$, we use the following result:

**Lemma 11.3** ([26])**.** *Let* $\Delta(\omega) = \omega^2 + K_1\omega + K_0$. *Suppose that* $\Delta(1) > 0$. *If* $\omega_1$ *and* $\omega_2$ *are solutions of* $\Delta(\omega) = 0$, *then*

*(1)* $|\omega_1| < 1$ *together with* $|\omega_2| < 1$ *if* $\Delta(-1) > 0 \wedge K_0 < 1$,

*(2)* $|\omega_1| < 1 \wedge |\omega_2| > 1$ *(or* $|\omega_1| > 1 \wedge |\omega_2| < 1$*) if* $\Delta(-1) < 0$,

*(3)* $|\omega_{1,2}| > 1$ *if* $\Delta(-1) > 0 \wedge K_0 > 1$,

*(4)* $|\omega_2| \neq 1$ *and* $\omega_1 = -1$ *if* $\Delta(-1) = 0$ *and* $K_1 \neq 0, 2$,

*(5)* $\omega_1, \omega_2 \in \mathbb{C}$ *along with* $|\omega_{1,2}| = 1$ *if* $K_1^2 - 4K_0 < 0 \wedge K_0 = 1$.

One can check that

$$J(E^*) = \begin{bmatrix} 1 + (-1 + a - ac^2)M & -ac^2M \\ b(-1+c)^2M & 1 + b(-1+c)cM \end{bmatrix}. \tag{11.4}$$

The corresponding characteristic polynomial is $\Delta(\omega) = \omega^2 + K_1\omega + K_0$, where

$$\begin{aligned} K_1 &= -2 + M - b(-1+c)cM + a(-1+c^2)M, \\ K_0 &= 1 + M(-1 + bc(-1 + c + M - cM) - a(-1+c)(1 + c + b(-1+c)cM)). \end{aligned}$$

It can be obtained through calculations that:

$$\begin{aligned} \Delta(0) &= 1 + M(-1 + bc(-1 + c + M - cM) - a(-1+c)(1 + c + b(-1+c)cM)), \\ \Delta(-1) &= 4 + 2(-1 + a + b(-1+c)c - ac^2)M - bcM^2(1 - a + ac)(-1+c), \\ \Delta(1) &= b(1 - a(1-c))(1-c)cM^2. \end{aligned}$$

Clearly, $\Delta(1) > 0$. By applying Lemma 11.3, we obtain the following result:

**Theorem 11.4.** $E^* = \left(1 - a(1-c), \frac{[1-a(1-c)](1-c)}{c}\right)$ *is*

*(1) a sink if* $a(1-c)(c+1+b(-1+c)cM) < 1 + bc(1-c-M+cM)$ *and* $a(2M - 2c^2M - b(-1+c)^2cM^2) > -4 + 2M + 2b(1-c)cM - b(1-c)cM^2$,

(2) *a source if* $a(1-c)(c+1+b(-1+c)cM) > 1+bc(1-c-M+cM)$ *and* $a(2M-2c^2M-b(-1+c)^2cM^2) > -4+2M+2b(1-c)cM-b(1-c)cM^2$,

(3) *a saddle if* $a(2M-2c^2M-b(-1+c)^2cM^2) < -4+2M+2b(1-c)cM-b(1-c)cM^2$,

(4) *non-hyperbolic, and* (10.7) *experiences a PD bifurcation at* $E_3$ *when* $-2+M-b(-1+c)cM+a(-1+c^2)M \neq 0, 2$ *and* $a(2M-2c^2M-b(-1+c)^2cM^2) = -4+2M+2b(1-c)cM-b(1-c)cM^2$,

(5) *non-hyperbolic, and* (10.7) *undergoes an NS bifurcation at* $E_3$ *when* $0 < M-b(-1+c)cM+a(-1+c^2)M < 4$ *and* $a(1-c)(c+1+b(-1+c)cM) = 1+bc(1-c-M+cM)$.

## 12. Bifurcation analysis

This section provides a thorough analysis of bifurcation, including PD and NS bifurcations, in (10.7) at the positive fixed point $E_2$. For a detailed theoretical background on bifurcation theory, readers are referred to [27–30]. Bifurcations are pivotal in understanding the qualitative behavior of dynamical systems, as even small parameter variations can lead to significant changes in system dynamics, particularly in prey–predator interactions. Comprehension of PD and NS bifurcations gives a deeper understanding of the dynamics of ecosystems and gives important insights for formulating efficient, sustainable management methods that provide for the continued coexistence of predator and prey populations. The study starts with the examination of the PD bifurcation at $E^*$ under condition (4) given in Theorem 11.4. By introducing a small perturbation $\xi$ to the bifurcation parameter $a$ near its critical value

$$a = \frac{-4+2M+2b(1-c)cM-b(1-c)cM^2}{2M-2c^2M-b(-1+c)^2cM^2},$$

model (10.7) takes the following form,

$$\begin{cases} x_{n+1} = x_n + M\Big(x_n(1-x_n) - \frac{(a+\xi)x_ny_n}{x_n+y_n}\Big), \\ y_{n+1} = y_n + M\Big(by_n(\frac{x_n}{x_n+y_n} - c)\Big). \end{cases} \tag{12.1}$$

We translate $E^*$ to the origin by using

$$u_n = x_n - 1 - (a+\xi)(1-c),\ v_n = y_n - \frac{[1-(a+\xi)(1-c)](1-c)}{c}.$$

Consequently, (12.1) can be rewritten as

$$\begin{bmatrix} u_{n+1} \\ v_{n+1} \end{bmatrix} = \begin{bmatrix} \frac{-2+c(-2+b(-1+c)(-1+c(-2+M))M)}{2+c(2+b(-1+c)M)} & \frac{c^2(-2+M)(2+b(-1+c)cM)}{-2+c(2c+b(-1+c)^2M)} \\ b(-1+c)^2M & 1+b(-1+c)cM \end{bmatrix} \begin{bmatrix} u_n \\ v_n \end{bmatrix} + \begin{bmatrix} \mathbb{F}_1(u_n, v_n, \xi) \\ \mathbb{F}_2(u_n, v_n, \xi) \end{bmatrix}, \tag{12.2}$$

where

$$\begin{aligned} \mathbb{F}_1(u_n, v_n, \xi) &= a_1u_n^2 + a_2v_n^2 + a_3u_nv_n + a_4u_n\xi + a_5v_n\xi + a_6u_n^3 + a_7v_n^3 + a_8u_n^2v_n \\ &\quad + a_9u_n^2\xi + a_{10}u_nv_n^2 + a_{11}v_n^2\xi + a_{12}u_nv_n\xi + O((|u_n|+|v_n|+|\xi|)^4), \\ \mathbb{F}_2(u_n, v_n, \xi) &= b_1u_n^2 + b_2v_n^2 + b_3u_nv_n + b_4u_n^3 + b_5v_n^3 + b_6u_n^2v_n + b_7u_n^2\xi + b_8u_nv_n^2 \\ &\quad + b_9v_n^2\xi + b_{10}u_nv_n\xi + O((|u_n|+|v_n|+|\xi|)^4). \end{aligned}$$

Appendix A provides the values of the coefficients $a_i$ and $b_j$. To diagonalize (12.2), we introduce the following transformation:

$$\begin{bmatrix} u_n \\ v_n \end{bmatrix} = \begin{bmatrix} -\frac{2-bcM+bc^2M}{b(-1+c)^2M} & -\frac{2c^2-c^2M}{(-1+c)(2+2c-bcM+bc^2M)} \\ 1 & 1 \end{bmatrix} \begin{bmatrix} e_n \\ f_n \end{bmatrix}. \tag{12.3}$$

Under the mapping (12.3), (12.2) is transformed as follows:

$$\begin{bmatrix} e_{n+1} \\ f_{n+1} \end{bmatrix} = \begin{bmatrix} -1 & 0 \\ 0 & \omega \end{bmatrix} \begin{bmatrix} e_n \\ f_n \end{bmatrix} + \begin{bmatrix} \mathbb{G}_1(e_n, f_n, \xi) \\ \mathbb{G}_2(e_n, f_n, \xi) \end{bmatrix}, \tag{12.4}$$

where

$$\begin{aligned}
\omega &= \frac{2 + c(2 + b(-1 + c)M(3 + (1 - b + bc))cM))}{2 + c(2 + bM(-1 + c))}, \\
\mathbb{G}_1(e_n, f_n, \xi) &= c_1 e_n^2 + c_2 f_n^2 + c_3 e_n f_n + c_4 e_n \xi + c_5 f_n \xi + c_6 e_n^3 + c_7 f_n^3 + c_8 e_n^2 f_n + c_9 e_n^2 \xi + c_{10} e_n f_n^2 \\
&\quad + c_{11} f_n^2 \xi + c_{12} e_n f_n \xi + O((|e_n|+|f_n|+|\xi|)^4), \\
\mathbb{G}_2(e_n, f_n, \xi) &= d_1 e_n^2 + d_2 f_n^2 + d_3 e_n f_n + d_4 e_n \xi + d_5 f_n \xi + d_6 e_n^3 + d_7 f_n^3 + d_8 e_n^2 f_n + d_9 e_n^2 \xi + d_{10} e_n f_n^2 \\
&\quad + d_{11} f_n^2 \xi + d_{12} e_n f_n \xi + O((|e_n|+|f_n|+|\xi|)^4).
\end{aligned}$$

Appendix B provides the values of the coefficients $c_i$ and $d_j$. Now, suppose that $\Sigma$ denotes the center manifold of (12.4), defined near the origin for $\xi$ close to zero. Its approximate form is given by

$$\Sigma = \Big\{(e_n, f_n, \xi) \in \mathbb{R}^3_+ \Big| f_n = p_1 e_n^2 + p_2 e_n \xi + p_3 \xi^2 + O((|e_n|+|\xi|)^3)\Big\}.$$

By calculations, we obtain $p_1 = \frac{d_1}{1-\omega}$, $p_2 = -\frac{d_4}{1+\omega}$, $p_3 = 0$. Thus, (12.4) limited to $\Sigma$ can be written as follows:

$$\begin{aligned}
\Upsilon := e_{n+1} &= -e_n + c_1 e_n^2 + c_4 e_n \xi + \Big(c_6 + \frac{c_3 d_1}{1-\omega}\Big) e_n^3 + \Big(c_9 + \frac{c_5 d_1}{1-\omega} - \frac{c_3 d_4}{1+\omega}\Big) e_n^2 \xi \\
&\quad - \Big(\frac{c_5 d_4}{1+\omega}\Big) e_n \xi^2 + O\Big((|e_n|+|\xi|)^4\Big).
\end{aligned} \tag{12.5}$$

For the mapping (12.5) to exhibit a PD bifurcation, it is required that the values $l_1$ and $l_2$ are non-zero, where

$$l_1 = \Upsilon_\xi \Upsilon_{e_n e_n} + 2\Upsilon_{e_n \xi}\Big|_{(0,0)} = 2c_4, \tag{12.6}$$

$$l_2 = \frac{1}{2}(\Upsilon_{e_n e_n})^2 + \frac{1}{3}\Upsilon_{e_n e_n e_n}\Big|_{(0,0)} = 2\Big(c_1^2 + c_6 + \frac{c_3 d_1}{1-\omega}\Big). \tag{12.7}$$

Thus, we get the subsequent result:

**Theorem 12.1.** *Suppose that condition* (4) *of Theorem 11.4 is satisfied. Then* (10.7) *experiences PD bifurcation at $E^*$ if $l_1, l_2$ listed in* (12.6) *and* (12.7) *are non-zero and a differs in a small neighborhood of*

$$a = \frac{-4 + 2M + 2b(1-c)cM - b(1-c)cM^2}{2M - 2c^2M - b(-1+c)^2cM^2}.$$

*Furthermore, if $l_2 > 0$ ($l_2 < 0$), a period-2 orbit of* (10.7) *bifurcates from $E^*$, which is stable (unstable).*

Now, we investigate the occurrence of the NS bifurcation at the equilibrium point $E^*$ based on condition (5) of Theorem 11.4. By introducing a minor disturbance $\xi$ into bifurcation parameter $a$ near its critical value

$$a = \frac{1 + bc(1 - c - M + cM)}{(c + 1 + b(-1 + c)cM)(1 - c)},$$

model (10.7) is transformed to

$$\begin{cases} x_{n+1} = x_n + M\Big(x_n(1 - x_n) - \frac{(a+\xi)x_n y_n}{x_n + y_n}\Big), \\ y_{n+1} = y_n + M\Big(by_n(\frac{x_n}{x_n + y_n} - c)\Big). \end{cases} \tag{12.8}$$

We shift $E^*$ to $(0, 0)$ by using

$$u_n = x_n - 1 - (a + \xi)(1 - c),\ v_n = y_n - \frac{[1 - (a + \xi)(1 - c)](1 - c)}{c}.$$

Consequently, (12.8) can be rewritten as

$$\begin{bmatrix} u_{n+1} \\ v_{n+1} \end{bmatrix} = \begin{bmatrix} j_{11} & -\frac{c^2M(-1+(-1+c^2)\xi+b(-1+c)c(1+M(-1+(-1+c)\xi)))}{(-1+c)(1+c-bcM+bc^2M)} \\ b(-1 + c)^2M & 1 + b(-1 + c)cM \end{bmatrix} \begin{bmatrix} u_n \\ v_n \end{bmatrix} + \begin{bmatrix} F(u_n, v_n) \\ G(u_n, v_n) \end{bmatrix}, \tag{12.9}$$

where

$$\begin{aligned} j_{11} &= \frac{1 + c^2M(b + bM(-1 + \xi) - \xi) + M\xi - bc^4M^2\xi + c(1 + M\xi - bM^2\xi) + c^3M(-\xi + b(-1 + M + M\xi))}{1 + c - bcM + bc^2M}, \\ F(u_n, v_n) &= a_1u_n^2 + a_2v_n^2 + a_3u_nv_n + a_4u_n^3 + a_5v_n^3 + a_6u_n^2v_n + a_7u_nv_n^2 + O((|u_n|+|v_n|)^4), \\ G(u_n, v_n) &= b_1u_n^2 + b_2v_n^2 + b_3u_nv_n + b_4u_n^3 + b_5v_n^3 + b_6u_n^2v_n + b_7u_nv_n^2 + O((|u_n|+|v_n|)^4). \end{aligned}$$

Appendix C provides the values of the coefficients $a_i$ and $b_j$. Evaluating the Jacobian matrix of (12.9) at $(0, 0)$, we obtain the following characteristic equation:

$$\omega^2 - p(\xi)\omega + q(\xi) = 0, \tag{12.10}$$

where

$$\begin{aligned} p(\xi) &= -\frac{1}{1 + c - bcM + bc^2M}\Big( - 2 - M\xi + bc^4M^2(-b + \xi) + c(-1 + bM)(2 + M\xi) \\ &\quad + c^3M(2b^2M + \xi - bM(1 + \xi)) + c^2M(-b^2M + \xi + b(-2 + M - M\xi))\Big), \\ q(\xi) &= 1 - b(-1 + c)^2cM^2\xi + M(\xi - c^2\xi). \end{aligned}$$

The solutions of (12.10) are

$$\omega_{1,2} = \frac{p(\xi)}{2} \pm \frac{i}{2}\sqrt{4q(\xi) - p^2(\xi)}. \tag{12.11}$$

We then obtain $|\omega_{1,2}| = \sqrt{q(\xi)}$. Furthermore,

$$\left(\frac{\mathrm{d}|\omega_1|}{\mathrm{d}\xi}\right)_{\xi=0} = \left(\frac{\mathrm{d}|\omega_2|}{\mathrm{d}\xi}\right)_{\xi=0} = -\frac{1}{2}(-1 + c)M(1 + c - bcM + bc^2M) \neq 0.$$

Additionally, it is required that $\omega_{1,2}^i \neq 1$ when $\xi = 0$ for $i = 1, 2, 3, 4$, corresponds to $p(0) \neq -2, 0, 1, 2$. We obtain that

$$p(0) = \frac{2 + (1-2b)bc^3M^2 + b^2c^4M^2 + bc^2M(2 + (-1+b)M) + c(2-2bM)}{1 + c - bcM + bc^2M} \neq \pm 2.$$

Thus, we only require that

$$\frac{2 + (1-2b)bc^3M^2 + b^2c^4M^2 + bc^2M(2 + (-1+b)M) + c(2-2bM)}{1 + c - bcM + bc^2M} \neq 0, 1. \tag{12.12}$$

To obtain the canonical form of (12.9) as $\xi = 0$, we use

$$\begin{bmatrix} u_n \\ v_n \end{bmatrix} = \begin{bmatrix} \frac{c^2(1+b(-1+c)c(-1+M))M}{(-1+c)(1+c-bcM+bc^2M)} & 0 \\ \frac{b(-1+c)cM(2+bc^2M-c(-2+M+bM))}{2(1+c-bcM+bc^2M)} & c_{22} \end{bmatrix} \begin{bmatrix} e_n \\ f_n \end{bmatrix}, \tag{12.13}$$

where

$$c_{22} = -\frac{1}{2}\sqrt{4 - \frac{(2 + (1-2b)bc^3M^2 + b^2c^4M^2 + bc^2M(2 + (-1+b)M) + c(2-2bM))^2}{(1 + c - bcM + bc^2M)^2}}.$$

Thus, we obtain

$$\begin{bmatrix} e_{n+1} \\ f_{n+1} \end{bmatrix} = \begin{bmatrix} k_{11} & c_{22} \\ -c_{22} & k_{11} \end{bmatrix} \begin{bmatrix} e_n \\ f_n \end{bmatrix} + \begin{bmatrix} \chi(e_n, f_n) \\ \Upsilon(e_n, f_n) \end{bmatrix}, \tag{12.14}$$

where

$$\begin{aligned} k_{11} &= \frac{2 + (1-2b)bc^3M^2 + b^2c^4M^2 + bc^2M(2 + (-1+b)M) + c(2-2bM)}{2(1 + c - bcM + bc^2M)}, \\ \chi(e_n, f_n) &= c_1e_n^2 + c_2f_n^2 + c_3e_nf_n + c_4e_n^3 + c_5f_n^3 + c_6e_n^2f_n + c_7e_nf_n^2 + O((|e_n|+|f_n|)^4), \\ \Upsilon(e_n, f_n) &= d_1e_n^2 + d_2f_n^2 + d_3e_nf_n + d_4e_n^3 + d_5f_n^3 + d_6e_n^2f_n + d_7e_nf_n^2 + O((|e_n|+|f_n|)^4). \end{aligned}$$

Appendix D provides the values of $c_i$ and $d_j$. To analyze the direction and nature of the NS bifurcation, the first Lyapunov exponent is evaluated as follows:

$$L = \left( \left[ -Re\left( \frac{(1-2\omega_1)\omega_2^2}{1-\omega_1}\tau_{20}\tau_{11} \right) - \frac{1}{2}|\tau_{11}|^2 - |\tau_{02}|^2 + Re(\omega_2\tau_{21}) \right] \right)_{\xi=0}, \tag{12.15}$$

where

$$\begin{aligned} \tau_{20} &= \frac{1}{8}\left[ \chi_{e_ne_n} - \chi_{f_nf_n} + 2\Upsilon_{e_nf_n} + i(\Upsilon_{e_ne_n} - \Upsilon_{f_nf_n} - 2\chi_{e_nf_n}) \right], \\ \tau_{11} &= \frac{1}{4}\left[ \chi_{e_ne_n} + \chi_{f_nf_n} + i(\Upsilon_{e_ne_n} + \Upsilon_{f_nf_n}) \right], \\ \tau_{02} &= \frac{1}{8}\left[ \chi_{e_ne_n} - \chi_{f_nf_n} - 2\Upsilon_{e_nf_n} + i(\Upsilon_{e_ne_n} - \Upsilon_{f_nf_n} + 2\chi_{e_nf_n}) \right], \\ \tau_{21} &= \frac{1}{16}\left[ \chi_{e_ne_ne_n} + \chi_{e_nf_nf_n} + \Upsilon_{e_ne_nf_n} + \Upsilon_{f_nf_nf_n} + i(\Upsilon_{e_ne_ne_n} + \Upsilon_{e_nf_nf_n} - \chi_{e_ne_nf_n} - \chi_{f_nf_nf_n}) \right]. \end{aligned}$$

The foregoing discussion leads to the following conclusion:

**Theorem 12.2.** *Suppose that condition* (5) *of Theorem 11.4 is fulfilled. If condition* (12.12) *is fulfilled and L, defined in* (12.15)*, is nonzero, then* (10.7) *experiences an NS bifurcation at $E^*$ when the parameter a differs in a small neighborhood of*

$$a = \frac{1 + bc(1 - c - M + cM)}{(1 - c)(1 + c + b(-1 + c)cM)}.$$

*Additionally, if $L < 0$ (respectively, $L > 0$), the NS bifurcation at $E^*$ is supercritical (respectively, subcritical), and a unique invariant closed curve emanates from $E^*$, the curve is attracting in the former case and repelling in the latter.*

## 13. Numerical simulations for discrete model (10.7)

In this section, we present numerical examples to support the analytical findings of the discrete fractional prey–predator model (10.7). The simulations illustrate how variations in system parameters lead to qualitative variations in the population dynamics, including the onset of periodic and chaotic behaviors via PD and NS bifurcations. The bifurcation diagrams, phase portraits, time series plots, and maximum Lyapunov exponents (MLEs) are used to characterize these transitions.

In the numerical simulations of the discrete model (10.7), two different settings are considered. First, in simulations where the effective discretization parameter is fixed, we choose $M = 3.5$, which is obtained by taking the fractional order $\sigma = 0.95$ and the sampling step size $\theta \approx 3.66$. In this case, the values of $\theta$ and $\sigma$ are kept constant throughout the simulations. Second, in simulations where $M$ is varied as a bifurcation parameter, we fix the fractional order $\sigma = 0.95$ and vary the sampling step size $\theta$ accordingly so that $M = \frac{\theta^\sigma}{\Gamma(\sigma+1)}$ changes continuously.

### *13.1. PD bifurcation analysis*

We fix $M = 3.5, b = 0.5$, and $c = 0.95$. The corresponding PD bifurcation value is $a \approx 4.30466$. At this bifurcation point, the interior fixed point is $E^* \approx (0.784767, 0.041304)$, where the prey and predator populations coexist at stable levels. The eigenvalues of $J(E^*)$ are $\omega_1 = -1$, $\omega_2 = 0.885841$. The emergence of the $-1$ eigenvalue verifies the existence of a PD bifurcation at this value. This implies a qualitative change in the dynamics of the system whereby the fixed point, which is stable initially, becomes unstable and bifurcates to a stable period of two orbits as the parameter $a$ increases.

To visualize this transition, we generate bifurcation diagrams in Figure 3(a),3(b), showing the asymptotic behavior of the prey and predator populations as $a$ varies over $[2.8, 4.8]$. The initial conditions are fixed at $x_0 = 0.75, y_0 = 0.05$. These plots show the successive PD behavior, with increasingly complicated oscillations and ultimately chaotic dynamics as $a$ goes down. Additionally, the corresponding MLE is plotted in Figure 3(c). Negative values for the MLE establish that the system has stable or periodic behavior in the early regime. As $a$ goes down and crosses the bifurcation point, the MLE turns positive, which shows the onset of chaotic behavior. This verifies that the system takes the classical PD path towards chaos.

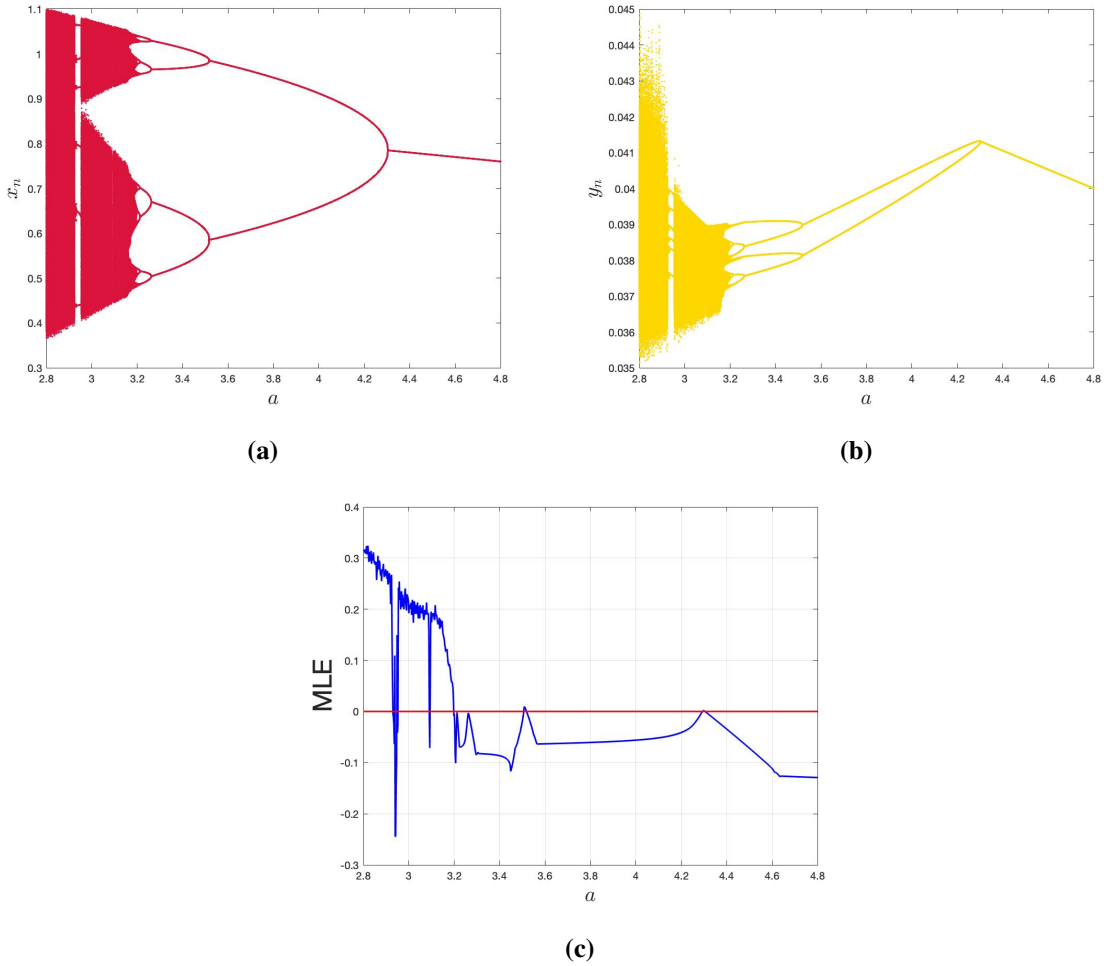


**(a)** **(b)**

**(c)**

**Figure 3.** Bifurcation and MLE graphs of (10.7) varying $a \in [2.8, 4.8]$ and fixing $M = 3.5, b = 0.5, c = 0.95$ with $x_0 = 0.75, y_0 = 0.05$.

To illustrate further the dynamic changes in the prey–predator model, we provide time series plots and phase portraits for certain values of $a$, using $M = 3.5, b = 0.5, c = 0.95$. These are Figures 4 and 5, and they show how the system transforms from stability to chaos via a cascade of PD bifurcations. Plots Figure 4(a)–4(c) is for values of $a$ slightly lower than the critical bifurcation point $a \approx 4.30466$, when the system is stable, and the population levels of both predator and prey settle into a steady equilibrium. Below this value of $a$, the fixed point becomes unstable, and a PD bifurcation sets in for the system. This switch is reflected in Figure 4(d)–4(f), in which the model follows a 2-period cycle, reflecting alternating population values over time. With further reduction in the parameter $a$, the model continues to bifurcate, yielding higher-order periodic orbits. Figure 4(g)–4(i),4(j)–4(l) reflects the appearance of 4-period and 8-period cycles, respectively, representing further steps in the PD cascade. Ultimately, the system reveals chaotic behavior as depicted in Figure 5(a)–5(f). In this regime, both the prey and predator populations vary irregularly, with no apparent periodicity, and phase portraits reveal a complex, aperiodic structure. These simulations clearly demonstrate the classical PD route to chaos. Instability at the fixed point resulting from a flip bifurcation triggers a series of bifurcations that give way to increasingly complicated dynamics and eventually to chaos. This sequence shows sensitivity to

the parameter values in the system and reaffirms the intricacy of the dynamical behavior of the model.

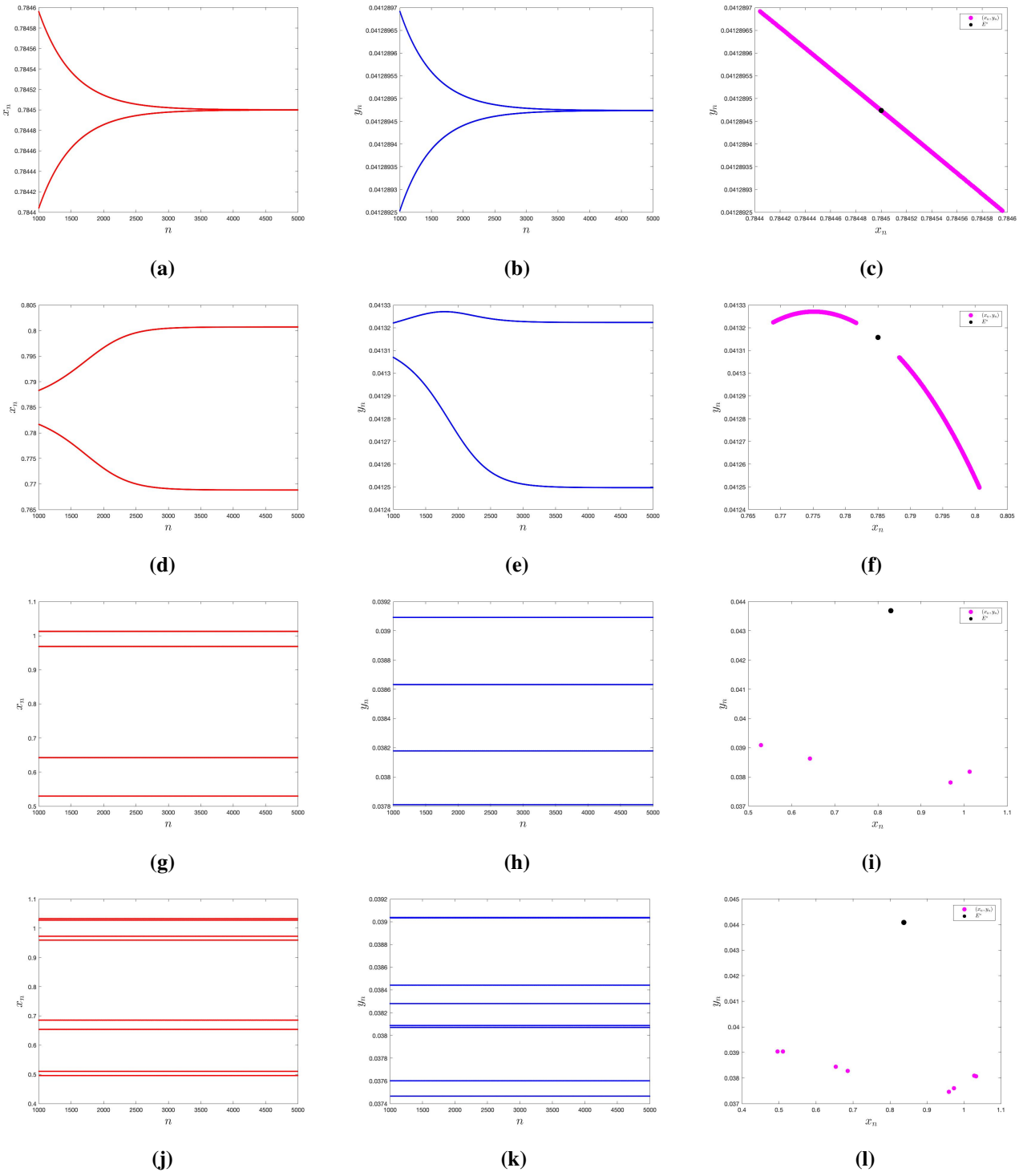


**Figure 4.** Time series plots and phase portraits of (10.7) using (a–c) $a = 4.31$, (d–f) $a = 4.30$, (g–i) $a = 3.40$, (j–l) $a = 3.25$ and fixing $M = 3.5, b = 0.5, c = 0.95$, with $x_0 = 0.75, y_0 = 0.05$.

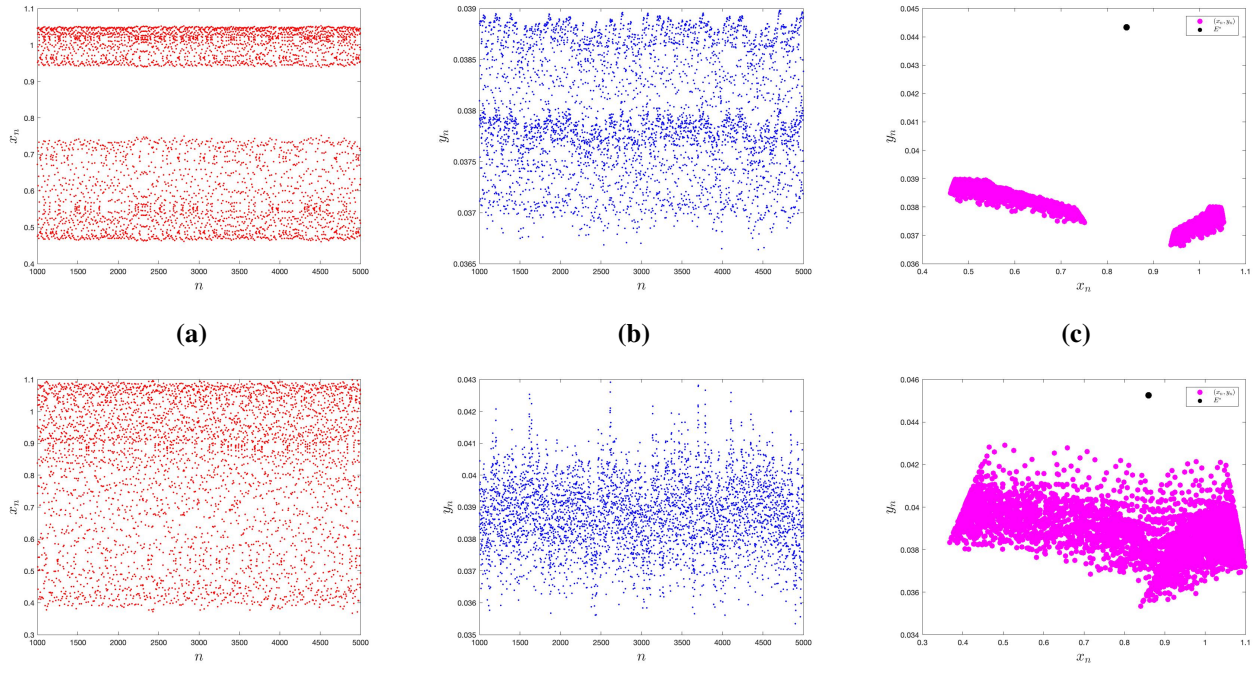

**(a)** **(b)** **(c)**

**(d)** **(e)** **(f)**

**Figure 5.** Time series plots and phase portraits of (10.7) using (a–c) $a = 3.15$, (d–f) $a = 2.8$ and fixing $M = 3.5, b = 0.5, c = 0.95$ with $x_0 = 0.75, y_0 = 0.05$.

In order to gain a more profound insight into the dynamics of the system when varying the different parameters, we study the bifurcation structure on the $(a, M)$ parameter plane. Figure 6(a) presents the two-parameter bifurcation diagram, which shows several dynamical behaviors such as stable fixed points, periodic orbits, and chaotic areas. The associated two-dimensional MLE plot in Figure 6(b) indicates the transition from negative to positive values, representing a change from stability to chaos.

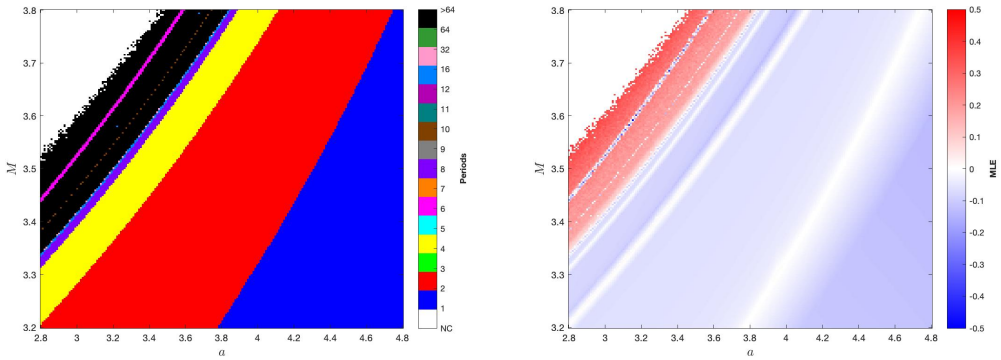

**(a)** **(b)**

**Figure 6.** 2D Bifurcation and 2D MLE plots of (10.7) varying at $a \in [2.8, 4.8]$ and $M \in [3.2, 3.8]$ and fixing $b = 0.5, c = 0.95$ with $x_0 = 0.75, y_0 = 0.05$.

*13.2. NS bifurcation analysis*

To investigate the presence of an NS bifurcation in the prey–predator model (10.7), we fix $M = 3.5, b = 0.92$, and $c = 0.45$. The corresponding NS bifurcation value is $a \approx 1.19927$. At this bifurcation point, the interior fixed point is $E^* \approx (0.340403, 0.416048)$. The eigenvalues of $J(E^*)$ are $\omega_{1,2} = 0.525253 \pm 0.850946i$, with modulus $|\omega_{1,2}| = 1$. This confirms the appearance of an NS bifurcation at $E^*$.

To capture this behavior, we draw bifurcation diagrams varying at $a \in [1.05, 1.30]$, as shown in Figure 7(a),7(b), using initial conditions $x_0 = 0.35, y_0 = 0.40$. The diagrams illustrate how the dynamics transition from stable, fixed-point behavior to quasiperiodic oscillations as $a$ crosses the bifurcation threshold. Further evidence is provided by the MLE plot in Figure 7(c). The negative values of MLE are showing stability or quasiperiodic behavior, and the absence of positive values showing NS bifurcation is not leading to chaos in our case.

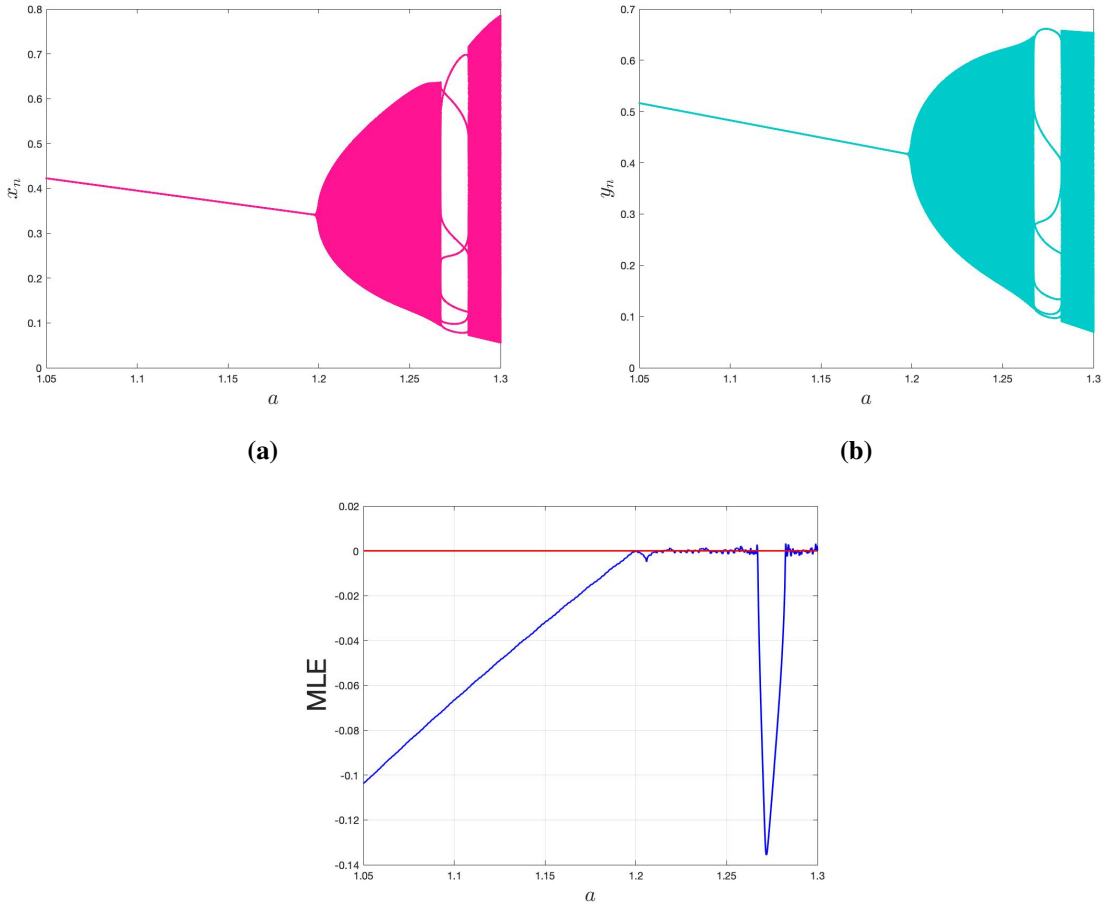


**(a)** **(b)**

**(c)**

**Figure 7.** Bifurcation and MLE plots of (10.7) varying $a \in [1.05, 1.30]$. Fixed values are $M = 3.5, b = 0.92, c = 0.45$, and initial values are $x_0 = 0.35, y_0 = 0.40$.

Figure 8 illustrates phase portraits of (10.7) for several values of $a$, capturing the evolution of dynamics near the NS bifurcation point. In Figure 8(a), for values of $a$ slightly below the critical threshold $a \approx 1.19927$, the positive fixed point $E^*$ behaves as a stable sink, with nearby trajectories spiraling toward it. As the parameter $a$ increases and crosses the bifurcation value, the fixed point becomes unstable, and an invariant closed curve is born through an NS bifurcation. This emergence is clearly observed in Figure 8(b)–8(d), where trajectories no longer converge to a point but instead settle onto a smooth closed orbit, indicating quasiperiodic behavior. Figure 8(g) presents a 3D visualization of these phase portraits, demonstrating the manner in which the radius of the invariant curve is expanding as the parameter $a$ increases further from the bifurcation threshold. This expansion of the orbit indicates that the amplitude of the oscillations of prey and predator populations increases with growing $a$. For $a = 1.27$, the smooth invariant curve destabilizes and splits into a period-7 periodic orbit, as presented in Figure 8(e). This is an indication of a secondary bifurcation, showing greater complication in the system's oscillatory behavior. Noticeably, as $a$ is increased further, the closed invariant curve returns, as illustrated in Figure 8(f), indicating a quasiperiodic regime to follow the intermittent periodic regime.

To investigate the global dynamical behavior associated with the NS bifurcation, we examine the system by varying the important parameters simultaneously. The two-parameter bifurcation diagram in the $(a, M)$ plane, shown in Figure 9(a), identifies different dynamic regions for stable fixed points, closed invariant curves, and quasiperiodic behavior. Figure 9(b) shows the respective two-dimensional MLE plot, which illustrates a transition from negative to positive values and marks the onset of quasiperiodic and chaotic dynamics. These plots combined confirm the presence of NS bifurcations and assist in explaining how changes in system parameters result in intricate dynamical patterns.

The numerical computations establish that the discrete prey–predator model has two main pathways to complexity: the PD and NS bifurcations. For different values of $a$, the system evolves from coexistence to periodic, quasiperiodic, and finally chaotic behavior. The bifurcation diagrams, Lyapunov exponents, and phase portraits together illustrate how the dynamics between predation pressure, conversion effectiveness, and memory terms ($M$ and $\sigma$) influence long-term population oscillations. These results emphasize that even modest alterations in rates of ecological interactions can produce large qualitative changes in system behavior, a demonstration of the inherent richness and sensitivity of discrete-time ecological dynamics.

### *13.3. A comparison of fractional-order and integer-order models*

To demonstrate the impact of fractional dynamics on system behavior, we compare the discretized fractional prey–predator model (10.7) with its classical integer-order counterpart, which is obtained by taking $\sigma = 1$. The parameters are set to $b = 0.92$, $c = 0.45$, and $\theta = 1$. The respective bifurcation plots are given in Figure 10.

On these plots, we can observe that the integer-order model has a wider region of stability than its fractional-order analogue. For the integer-order model, bifurcation happens at a greater critical value of $a$, and the model has steady coexistence over a larger range of parameters. The fractional-order model, in contrast, has a much earlier emergence of oscillations and bifurcations and exhibits more irregular and complex dynamics.

This comparison emphasizes that the memory effect inherent in fractional-order systems markedly changes the dynamical response, increasing sensitivity to parameter changes and generating richer

oscillatory and quasiperiodic dynamics. Such effects reflect the ability of fractional calculus to capture long-term memory and hereditary characteristics in population interactions, offering a more realistic description of ecological processes.

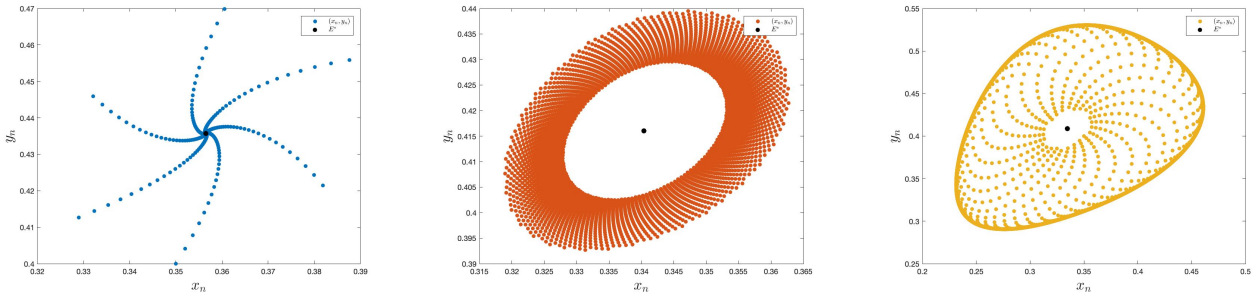

**(a)** $a = 1.17$ **(b)** $a = 1.1993$ **(c)** $a = 1.21$

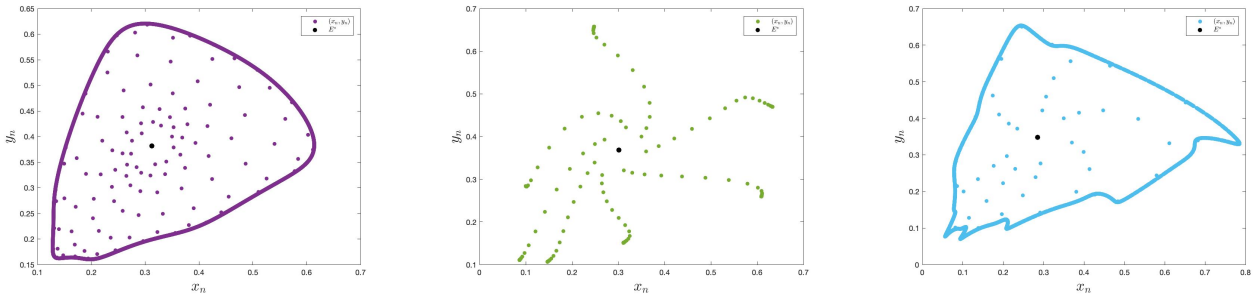

**(d)** $a = 1.25$ **(e)** $a = 1.27$ **(f)** $a = 1.30$

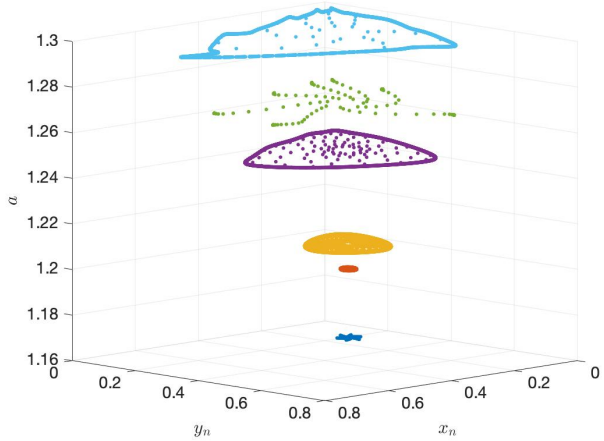


**(g)** 3D view of phase portraits

**Figure 8.** Phase portraits of (10.7) for some values of $a$ with $M = 3.5, b = 0.92, c = 0.45$, and $x_0 = 0.35, y_0 = 0.40$.

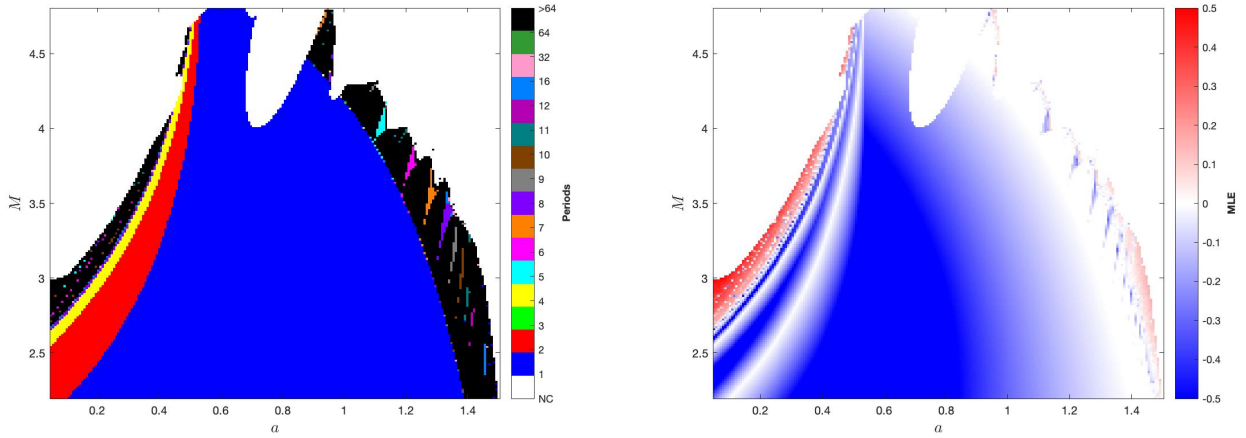


**(a)** **(b)**

**Figure 9.** 2D Bifurcation and 2D MLE graphs of (10.7) varying at $a \in [0.05, 1.5]$ and $M \in [2.2, 4.8]$. Fixing $b = 0.92, c = 0.45$ and $x_0 = 0.35, y_0 = 0.40$.

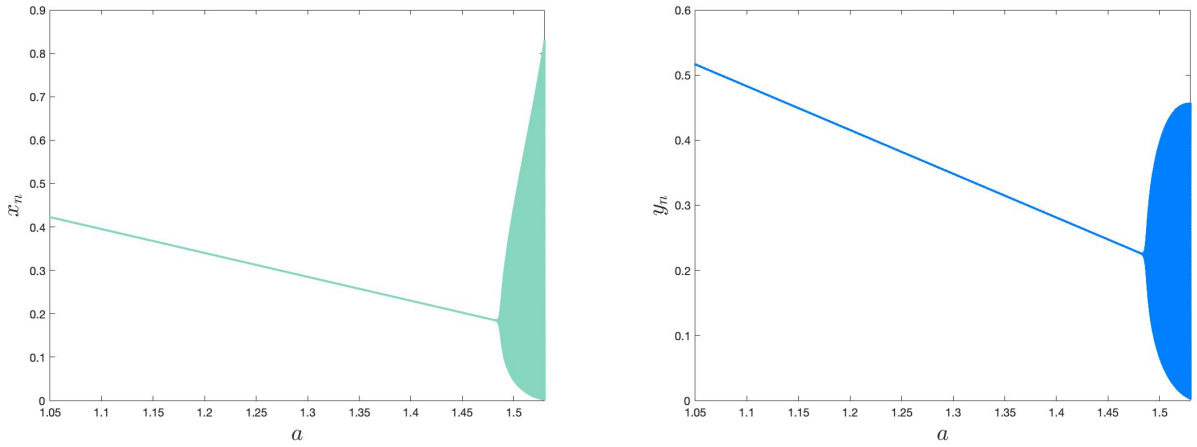


**(a)** **(b)**

**Figure 10.** Bifurcation diagrams of (10.7) varying $a$ in [1.05, 1.53]. and fixing $b = 0.92, c = 0.45, \theta = 1, \sigma = 1$, and $x_0 = 0.35, y_0 = 0.40$.

## 14. Conclusions

In this study, we developed and analyzed a fractional prey–predator model with a ratio-dependent functional response to capture the memory and hereditary effects in population interactions. The existence, uniqueness, positivity, and boundedness of biologically meaningful solutions were established, ensuring the well-posedness of the model. The local and global stability analyses demonstrated that both the predator-free and coexistence equilibria can achieve asymptotic stability under appropriate parameter conditions. The fractional order $\sigma$ was shown to play a crucial role in system dynamics, where smaller values of $\sigma$ enhance damping effects and suppress oscillations.

The Hopf bifurcation event was described by taking $\sigma$ as the bifurcation parameter, which showed how the memory terms affect the emergence of oscillations. To consider discrete-time dynamics, the piecewise constant argument method was used to obtain a discrete counterpart of the fractional system. The discrete model had a much more complex dynamical structure, such as PD and NS bifurcations toward complex periodic and quasiperiodic oscillations.

Numerical simulations, including bifurcation diagrams, phase portraits, and Lyapunov exponents, were used to verify the theoretical results and show the routes to chaos. Comparison with the integer-order model underscored that fractional dynamics cause earlier bifurcations and more intricate oscillatory behavior, stressing the effect of memory on ecological stability.

The research fills the gap between continuous fractional dynamics and discrete-time evolution, yielding further understanding of how discretization and memory act together to determine long-term population dynamics. The findings show that the combination of fractional-order modeling and discrete-time analysis provides a very effective method for analyzing complex ecological systems. Further research could explore extensions of the current fractional-order model by including time delays, stochastic influences, harvesting, or data-informed parameter estimation to strengthen its ecological relevance.

## Author contributions

Ibrahim Alraddadi: Conceptualization, Investigation, Methodology, Software, Writing – original draft. Ramesh Perumal: Formal analysis, Methodology, Validation, Visualization, Writing – review and editing. Rizwan Ahmed: Investigation, Methodology, Validation, Writing – original draft. Jawad Khan: Formal analysis, Software, Supervision, Visualization, Writing – review and editing. Youngmoon Lee: Investigation, Software, Supervision, Visualization, Writing – review and editing. All authors have read and approved the final version of the paper.

## Use of Generative-AI tools declaration

The authors declare they have not used Artificial Intelligence (AI) tools in the creation of this article.

## Acknowledgements

This work was supported in part by Institute of Information and Communications Technology Planning and Evaluation (IITP) grant IITP-2025-RS-2020-II201741, RS-2024-00423071 and National Research Foundation of Korea (NRF) BK21 grant Education/Research/Industry-Centric physical AI: ERICA all funded by the Korea government (MSIT, MOE).

## Conflict of interest

The authors have no conflicts of interest.

## References


1. A. J. Lotka, Elements of physical biology, *Nature*, **116** (1925), 461. https://doi.org/10.1038/116461b0
2. V. Volterra, Fluctuations in the abundance of a species considered mathematically, *Nature*, **118** (1926), 558–560. https://doi.org/10.1038/118558a0
3. M. Javidi, N. Nyamoradi, Dynamic analysis of a fractional order prey-predator interaction with harvesting, *Appl. Math. Model.*, **37** (2023), 8946-8956. https://doi.org/10.1016/j.apm.2013.04.024
4. H. L. Li, L. Zhang, C. Hu, Y. L. Jiang, Z. Teng, Dynamical analysis of a fractional-order predator-prey model incorporating a prey refuge, *J. Appl. Math. Comput.*, **54** (2017), 435–449. https://doi.org/10.1007/s12190-016-1017-8
5. M. F. Elettreby, A. A. Al-Raezah, T. Nabil, Fractional-order model of two-prey one-predator system, *Math. Probl. Eng.*, **2017** (2017), 6714538. https://doi.org/10.1155/2017/6714538
6. H. L. Li, A. Muhammadhaji, L. Zhang, Z. Teng, Stability analysis of a fractional-order predator-prey model incorporating a constant prey refuge and feedback control, *Adv. Differ. Equ.*, **2018** (2018), 325. https://doi.org/10.1186/s13662-018-1776-7
7. K. Sarkar, B. Mondal, Dynamic analysis of a fractional-order predator-prey model with harvesting, *Int. J. Dynam. Control*, **11** (2023), 1518–1531. https://doi.org/10.1007/s40435-022-01074-5
8. G. Zhang, Y. Shen, B. Chen, Positive periodic solutions in a non-selective harvesting predator-prey model with multiple delays, *J. Math. Anal. Appl.*, **395** (2012), 298–306. https://doi.org/10.1016/j.jmaa.2012.05.045
9. G. Zhang, Y. Shen, B. Chen, Hopf bifurcation of a predator-prey system with predator harvesting and two delays, *Nonlinear Dyn.*, **73** (2013), 2119–2131. https://doi.org/10.1007/s11071-013-0928-2
10. D. Midya, B. Bhunia, T. K. Kar, Influence of prey refuge and fear effect on fractional order delayed predator-prey model, *Phys. Scr.*, **100** (2025), 055212. https://doi.org/10.1088/1402-4896/adc849
11. B. Ghosh, B. Barman, M. Saha, Multiple dynamics in a delayed predator-prey model with asymmetric functional and numerical responses, *Math. Methods Appl. Sci.*, **46** (2023), 5187–5207. https://doi.org/10.1002/mma.8825
12. F. Alsharif, R. Ahmed, I. Alraddadi, M. Alsubhi, M. Amer, M. J. Uddin, A study of stability and bifurcation in a discretized predator-prey model with Holling type III response and prey refuge via piecewise constant argument method, *Complexity*, **2025** (2025), 4542190. https://doi.org/10.1155/cplx/4542190
13. P. A. Naik, Y. Javaid, R. Ahmed, Z. Eskandari, A. H. Ganie, Stability and bifurcation analysis of a population dynamic model with Allee effect via piecewise constant argument method, *J. Appl. Math. Comput.*, **70** (2024), 4189–4218. https://doi.org/10.1007/s12190-024-02119-y
14. R. Ahmed, A. Q. Khan, M. Amer, A. Faizan, I. Ahmed, Complex dynamics of a discretized predator-prey system with prey refuge using a piecewise constant argument method, *Int. J. Bifurcat. Chaos*, **34** (2024), 2450120. https://doi.org/10.1142/s0218127424501207

15. R. Ahmed, M. Adnan, A. Rauf, Dynamic complexity in a discretized fractional-order Cournot Duopoly model using piecewise constant argument method, *Quantum Inf. Process.*, **24** (2025), 256. https://doi.org/10.1007/s11128-025-04882-8

16. A. A. Kilbas, H. M. Srivastava, J. Trujillo, *Theory and applications of fractional differential equations*, Vol. 204, North-Holland Mathematics Studies, Elsevier, 2006. https://doi.org/10.1016/s0304-0208(06)x8001-5

17. Z. M. Odibat, N. T. Shawagfeh, Generalized Taylor's formula, *Appl. Math. Comput.*, **186** (2007), 286–293. https://doi.org/10.1016/j.amc.2006.07.102

18. I. Petráš, *Fractional-order nonlinear systems: modeling, analysis and simulation*, Springer Berlin, 2011. https://doi.org/10.1007/978-3-642-18101-6

19. Y. Li, Y. Q. Chen, I. Podlubny, Stability of fractional-order nonlinear dynamic systems: Lyapunov direct method and generalized Mittag-Leffler stability, *Comput. Math. Appl.*, **59** (2010), 1810–1821. https://doi.org/10.1016/j.camwa.2009.08.019

20. C. Vargas-De-Léon, Volterra-type Lyapunov functions for fractional-order epidemic systems, *Commun. Nonlinear Sci. Numer. Simul.*, **24** (2015), 75–85. https://doi.org/10.1016/j.cnsns.2014.12.013

21. B. Tang, Dynamics for a fractional-order predator-prey model with group defense, *Sci. Rep.*, **10** (2020), 4906. https://doi.org/10.1038/s41598-020-61468-3

22. M. S. Abdelouahab, N. E. Hamri, J. Wang, Hopf bifurcation and chaos in fractional-order modified hybrid optical system, *Nonlinear Dyn.*, **69** (2012), 275–284. https://doi.org/10.1007/s11071-011-0263-4

23. X. Li, R. Wu, Hopf bifurcation analysis of a new commensurate fractional-order hyperchaotic system, *Nonlinear Dyn.*, **78** (2014), 279–288. https://doi.org/10.1007/s11071-014-1439-5

24. K. Diethelm, N. J. Ford, A. D. Freed, A predictor-corrector approach for the numerical solution of fractional differential equations, *Nonlinear Dyn.*, **29** (2002), 3–22. https://doi.org/10.1023/a:1016592219341

25. E. Ahmed, A. M. El-Sayed, A. E. El-Mesiry, H. A. El-Saka, Numerical solution for the fractional replicator equation, *Int. J. Mod. Phys. C*, **16** (2011), 1017–1025. https://doi.org/10.1142/s0129183105007698

26. A. C. J. Luo, *Regularity and complexity in dynamical systems*, Vol. 1, Springer New York, 2012. https://doi.org/10.1007/978-1-4614-1524-4

27. J. Guckenheimer, P. Holmes, *Nonlinear oscillations, dynamical systems, and bifurcations of vector fields*, Vol. 42, Springer New York, 1983. https://doi.org/10.1007/978-1-4612-1140-2

28. S. Wiggins, M. Golubitsky, *Introduction to applied nonlinear dynamical Systems and Chaos*, Vol. 2. Springer New York, 2003. https://doi.org/10.1007/b97481

29. A. Suleman, A. Q. Khan, R. Ahmed, Bifurcation analysis of a discrete Leslie-Gower predator-prey model with slow-fast effect on predator, *Math. Methods Appl. Sci.*, **47** (2024), 8561–8580. https://doi.org/10.1002/mma.10032

30. A. Tassaddiq, A. Mehmood, R. Ahmed, Impact of carrying capacity on the dynamics of a discrete-time plant-herbivore system, *Chaos Soliton. Fract.*, **201** (2025), 117284. https://doi.org/10.1016/j.chaos.2025.117284

## Appendix

*A. List of coefficients associated with the nonlinear terms of* (12.2)

$$
\begin{aligned}
a_1 &= \frac{M(-4 + c(-4 + 2bM + c(4 + M(-2 + 2b(-2 + c)c - b(-1 + c)^2M))))}{4 + 2(1 + b(-1 + c))cM},\\
a_2 &= -\frac{c^3(-2 + M)M(2 + b(-1 + c)cM)}{2(-1 + c)(2 + (1 + b(-1 + c))cM)},\\
a_3 &= -\frac{c^2(-2 + M)M(2 + b(-1 + c)cM)}{2 + (1 + b(-1 + c))cM},\\
a_4 &= M - c^2M,\ a_5 = -c^2M,\\
a_6 &= \frac{(-1 + c)c^2(-2 + M)M^2(2 + b(-1 + c)cM)(2 + c(2 + b(-1 + c)M))}{4(2 + (1 + b(-1 + c))cM)^2},\\
a_7 &= \frac{c^4(-2 + M)M^2(2 + b(-1 + c)cM)(2 + c(2 + b(-1 + c)M))}{4(-1 + c)(2 + (1 + b(-1 + c))cM)^2},\\
a_8 &= \frac{c^2(-1 + 3c)(-2 + M)M^2(2 + bcM(c - 1))(2 + c(2 + b(-1 + c)M))}{4(2 + (1 + b(-1 + c))cM)^2},\\
a_9 &= \frac{cM^3(-2 + c(2c + b(-1 + c)^2M))^2}{4(2 + (1 + b(-1 + c))cM)^2},\\
a_{10} &= \frac{c^3(-2 + 3c)(-2 + M)M^2(2 + bcM(c - 1))(2 + c(2 + b(-1 + c)M))}{4(-1 + c)(2 + (1 - b + bc))cM)^2},\\
a_{11} &= \frac{c^3M^3(2 + c(2 + b(-1 + c)M))^2}{4(2 + (1 + b(-1 + c))cM)^2},\\
a_{12} &= \frac{(c - 1)c^2M^3(2 + c(2 + b(-1 + c)M))^2}{2(2 + (1 + b(-1 + c))cM)^2},\\
b_1 &= -\frac{b(-1 + c)^2cM^2(2 + c(2 + b(-1 + c)M))}{4 + 2(1 + b(-1 + c))cM},\\
b_2 &= -\frac{bc^3M^2(2 + c(2 + bM(-1 + c)))}{4 + 2(1 + b(-1 + c))cM},\\
b_3 &= -\frac{b(-1 + c)c^2M^2(2 + c(2 - bM + bcM))}{2 + (1 + b(-1 + c))cM},\\
b_4 &= \frac{bc^2M^3(-2 + c(2c + bM(c - 1)^2))^2}{4(2 + (1 + b(-1 + c))cM)^2},\\
b_5 &= \frac{bc^4M^3(2 + c(2 - bM + bcM))^2}{4(2 + (1 + b(-1 + c))cM)^2},
\end{aligned}
$$

$$b_6 = \frac{b(-1+c)c^2(-1+3c)M^3(2+c(2+bM(-1+c)))^2}{4(2+(1+b(-1+c))cM)^2},$$
$$b_7 = \frac{b(c-1)^3cM^3(2+c(2+b(-1+c)M))^2}{4(2+(1+b(-1+c))cM)^2},$$
$$b_8 = \frac{bc^3(-2+3c)M^3(2+c(2+b(-1+c)M))^2}{4(2+(1+b(-1+c))cM)^2},$$
$$b_9 = \frac{b(-1+c)c^3M^3(2+c(2+b(-1+c)M))^2}{4(2+(1+b(-1+c))cM)^2},$$
$$b_{10} = \frac{bc^2M^3(-2+c(2c+b(-1+c)^2M))^2}{2(2+(1+b(-1+c))cM)^2}.$$

*B. List of coefficients associated with the nonlinear terms of* (12.4)

$$\begin{aligned}
c_1 &= \Big(16+c(32-32bM+c(-16c+8(1+c+b(-1+5c))M+4b(-1+c)(1+2c+2b(-3+c+2c^2))M^2 \\
&\quad +2b^2(c-1)^2c(2+c+b(c-1)(4+c))M^3+b^3(1+b(c-1))(c-1)^3c^2M^4))\Big) \\
&\quad \Big/\Big(b(-1+c)^2(2+(1+b(-1+c))cM)(4+c(4+b(-1+c)M(4+(1+b(-1+c))cM)))\Big), \\
c_2 &= -\frac{bc^3(-2+M)M^2(4+cM(-2c+b(c-1)(4+c(-2+M+b(c-1)M))))}{16+2c(16-12bM+c(8+bM(12c+2(c-1)(1+c+b(c-1)(3+c))M+b(1+b(c-1))(-1+c)^2cM^2)))}, \\
c_3 &= -\frac{4c^3(-2+M)M}{-4+c(4c+4b(-1+c)^2M+b(1+b(-1+c))(-1+c)^2cM^2)}, \\
c_4 &= -\frac{(-1+c)M(2+c(2+b(-1+c)M))^2}{4+c(4+b(-1+c)M(4+(1+b(-1+c))cM))}, \\
c_5 &= \frac{b(-1+c)^2c^2(1+c+b(-1+c)c)M^3}{4+c(4+b(-1+c)M(4+(1+b(-1+c))cM))}, \\
c_6 &= -\frac{c^2(-2+M)(2+b(c-1)M)(-2+bcM)(2+c(2+b(-1+c)M))^2}{b^2(-1+c)^3(2+(1-b+bc)cM)^2(4+c(4+b(-1+c)M(4+(1+b(-1+c))cM)))}, \\
c_7 &= \frac{bc^4(-2+M)M^3(-2+bcM)(-2+cM(b(c-1)^2+c))}{32+4c(16-12bM+c(8+bM(12c+2(-1+c)(1+c+b(c-1)(3+c))M+b(1+b(c-1))(c-1)^2cM^2)))}, \\
c_8 &= \Big(c^2M(-2+M)(2+c(2+bM(c-1)))(4+c(-8+cM(-6+b(8+(2-3b)M+c(-6+M+bM(2 \\
&\quad +c+(1-b+bc)(-1+c)M)))))\Big) \\
&\quad \Big/\Big(b(-1+c)^2(2+(1+b(c-1))cM)^2(4+c(4+b(-1+c)M(4+(1+b(-1+c))cM)))\Big), \\
c_9 &= -\frac{cM^2(2+c(2+2bc-bM))(2+c(2+b(-1+c)M))^2}{b(2+(1-b+bc)cM)^2(4+c(4+b(-1+c)M(4+(1+b(-1+c))cM)))}, \\
c_{10} &= -\Big(\Big(c^3(-2+M)M^2(16+c(-8-12cM+bM(-12+c(2(10+M) \\
&\quad +c(-12+(1+b(-1+c))M(4+b(-1+c)M)))))\Big) \\
&\quad \Big/\Big(4(-8+c(8c+4(c-1)(c+1+b(c-1)(3+c))M \\
&\quad +6b(1+b(-1+c))(-1+c)^2cM^2+b(1+b(-1+c))^2(-1+c)^2c^2M^3))\Big)\Big), \\
c_{11} &= -\frac{b(c-1)^2c^3M^4(2+c(2+2bc-bM))}{4(4+c(4+b(-1+c)M(4+(1+b(-1+c))cM)))}, \\
c_{12} &= \frac{(-1+c)c^2M^3(2+c(2+2bc-bM))(2+c(2+b(-1+c)M))}{8+c(8+4M(1+c)+bM(c-1)(12+c(4+(1+b(-1+c))M(6+(1+b(-1+c))cM))))},
\end{aligned}$$

$$d_1 = -\frac{(2+bcM(c-1))(2+c(2+b(-1+c)M))(4+c(2+b(-1+c)M)(4+(1-b+bc)cM))}{b(-1+c)^2(2+(1+b(-1+c))cM)(4+c(4+b(-1+c)M(4+(1+b(-1+c))cM)))},$$

$$d_2 = \Big(bc^3M^2(-8(2+c)-4(-1+c)(1+5bc)M-2c(c+b(c-1)(-2+(5+4b(c-1))c))M^2 - b(1+b(-1+c))(-1+c)^2c^2(1+bc)M^3)\Big) \Big/\Big(16+2c(16-12bM+c(8+bM(12c+2(c-1)(1+c+b(c-1)(3+c))M + b(1-b+bc)(-1+c)^2cM^2)))\Big),$$

$$d_3 = \frac{2c^2M(2+(1+b(c-1))cM)(2+bcM(c-1))}{-4+c(4c+4b(-1+c)^2M+b(1-b+bc)(-1+c)^2cM^2)},$$

$$d_4 = \frac{(-1+c)M(2+c(2+b(-1+c)M))^2}{4+c(4+bM(c-1)(4+(1+b(-1+c))cM))},$$

$$d_5 = -\frac{b(-1+c)^2c^2(1+c+b(-1+c)c)M^3}{4+c(4+b(-1+c)M(4+(1+b(-1+c))cM))},$$

$$d_6 = -\frac{c^2(2+b(c-1)M)(2+b(c-1)cM)(4+(-1+c)(1+bc)M)(2+c(2+b(-1+c)M))^2}{b^2(-1+c)^4(2+(1-b+bc)cM)^2(4+c(4+b(-1+c)M(4+(1+b(c-1))cM)))},$$

$$d_7 = \Big(bc^4M^3(2+b(-1+c)cM)(-2+c(b(-1+c)^2+c)M)(4+M(c-1)(1+bc))\Big) \Big/\Big(4(-1+c)(8+c(16-12bM+c(8+bM(12c+2(c-1)(c+1+b(-1+c)(3+c))M + b(1-b+bc)(-1+c)^2cM^2)))\Big),$$

$$d_8 = \Big(c^2M(2+b(-1+c)cM)(4+(-1+c)(1+bc)M)(2+c(2+b(-1+c)M))(-2+c(4+3cM + b(-1+c)M(1+c(3+M+bM(c-1)))))\Big) \Big/\Big(b(-1+c)^3(2+(1+b(-1+c))cM)^2(4+c(4+b(-1+c)M(4+(1-b+bc)cM)))\Big),$$

$$d_9 = \frac{cM(2+(-1+c)(1+bc)M)(2+cM(2+b(c-1)))^3}{b(-1+c)(2+(1+b(-1+c))cM)^2(4+c(4+b(-1+c)M(4+(1+b(-1+c))cM)))},$$

$$d_{10} = -\Big(\Big(c^3M^2(2+b(-1+c)cM)(4+(-1+c)(1+bc)M) (-8+c(4+6cM+b(-1+c)M(-2+c(6+M+bM(c-1)))))\Big) \Big/\Big(4(-1+c)^2(8+c(8+4(1+c)M+b(-1+c)M(12+c(4+(1+b(-1+c))M(6+(1+b(-1+c))cM)))))\Big)\Big),$$

$$d_{11} = \frac{b(c-1)c^3M^3(2+(-1+c)(1+bc)M)(2+cM(2+b(c-1)))}{4(4+c(4+b(-1+c)M(4+(1+b(-1+c))cM)))},$$

$$d_{12} = -\frac{c^2M^2(2+(-1+c)(1+bc)M)(2+c(2+b(-1+c)M))^2}{8+c(8+4(1+c)M+b(-1+c)M(12+c(4+(1+b(-1+c))M(6+(1+b(-1+c))cM))))}.$$

### *C. List of coefficients associated with the nonlinear terms of* (12.9)

$$a_1 = \frac{M(\xi+c\xi-c^3\xi+c^4\xi-c^2(1+2\xi)+b(-1+c)c(-1-c+cM+M\xi+c^3M\xi-c^2(-1+M+2M\xi)))}{c-\xi+bc^3M\xi+bc(-1+M\xi)+c^2(b+\xi-2bM\xi)},$$

$$a_2 = \frac{c^3M(-1+(-1+c^2)\xi+bc(-1+c)(1+M(-1+(c-1)\xi)))}{(-1+c)(c-\xi+bc^3M\xi+bc(-1+M\xi)+c^2(b+\xi-2bM\xi))},$$

$$a_3 = \frac{2c^2M(-1+(-1+c^2)\xi+bc(-1+c)(1+M(-1+(c-1)\xi)))}{c-\xi+bc^3M\xi+bc(-1+M\xi)+c^2(b+\xi-2bM\xi)},$$

$$a_4 = -\frac{(-1+c)c^2M(1+c-bcM+bc^2M)(-1+(-1+c^2)\xi+b(-1+c)c(1+M(-1+(-1+c)\xi)))}{(c-\xi+bc^3M\xi+bc(-1+M\xi)+c^2(b+\xi-2bM\xi))^2},$$

$$a_5 = -\frac{c^4M(1+c-bcM+bc^2M)(-1+(-1+c^2)\xi+bc(c-1)(1+M(-1+(-1+c)\xi)))}{(-1+c)(c-\xi+bc^3M\xi+bc(-1+M\xi)+c^2(b+\xi-2bM\xi))^2},$$

$$a_6 = -\frac{c^2M(3c-1)(1+c-bcM+bc^2M)(-1+(-1+c^2)\xi+bc(c-1)(1+M(-1+(-1+c)\xi)))}{(c-\xi+bc^3M\xi+bc(-1+M\xi)+c^2(b+\xi-2bM\xi))^2},$$

$$a_7 = -\frac{c^3M(3c-2)(1+c-bcM+bc^2M)(-1+(-1+c^2)\xi+b(-1+c)c(1+M(-1+(c-1)\xi)))}{(-1+c)(c-\xi+bc^3M\xi+bc(-1+M\xi)+c^2(b+\xi-2bM\xi))^2},$$

$$b_1 = -\frac{b(-1+c)^2cM(1+c-bcM+bc^2M)}{c-\xi+bc^3M\xi+bc(-1+M\xi)+c^2(b+\xi-2bM\xi)},$$

$$b_2 = -\frac{bc^3M(1+c-bcM+bc^2M)}{c-\xi+bc^3M\xi+bc(-1+M\xi)+c^2(b+\xi-2bM\xi)},$$

$$b_3 = -\frac{2b(-1+c)c^2M(1+c-bcM+bc^2M)}{c-\xi+bc^3M\xi+bc(-1+M\xi)+c^2(b+\xi-2bM\xi)},$$

$$b_4 = \frac{b(-1+c)^2c^2M(1+c-bcM+bc^2M)^2}{(c-\xi+bc^3M\xi+bc(-1+M\xi)+c^2(b+\xi-2bM\xi))^2},$$

$$b_5 = \frac{bc^4M(1+c-bcM+bc^2M)^2}{(c-\xi+bc^3M\xi+bc(-1+M\xi)+c^2(b+\xi-2bM\xi))^2},$$

$$b_6 = \frac{b(-1+c)c^2(-1+3c)M(1+c-bcM+bc^2M)^2}{(c-\xi+bc^3M\xi+bc(-1+M\xi)+c^2(b+\xi-2bM\xi))^2},$$

$$b_7 = \frac{bc^3(-2+3c)M(1+c-bcM+bc^2M)^2}{(c-\xi+bc^3M\xi+bc(-1+M\xi)+c^2(b+\xi-2bM\xi))^2}.$$

*D. List of coefficients associated with the nonlinear terms of* (12.14)

$$c_1 = -\frac{c^2M^2(4c+b^3(-1+c)^4c^2M^2+b^2(-1+c)^3cM(4+cM)+4b(-1+c)(-1+c^2M))}{4(-1+c)(1+c-bcM+bc^2M)},$$

$$c_2 = \frac{b(-1+c)c^2M^2(4+(1-2b)bc^3M^2+b^2c^4M^2+bc^2M(4+(-1+b)M)+c(4-4bM))}{4(1+c-bcM+bc^2M)},$$

$$c_3 = \frac{1}{2}cM(2+b(-1+c)cM)\sqrt{4-\frac{(2+(1-2b)bc^3M^2+b^2c^4M^2+bc^2M(2+(-1+b)M)+c(2-2bM))^2}{(1+c-bcM+bc^2M)^2}},$$

$$c_4 = \frac{c^3M^3(2+bcM(c-1))^2(2c+b^2(-1+c)^3cM+b(-1+c)(-2+cM+c^2M))}{8(-1+c)(1+c-bcM+bc^2M)},$$

$$c_5 = -\frac{c^2(1+c-bcM+bc^2M)^2(4-\frac{(2+(1-2b)bc^3M^2+b^2c^4M^2+bc^2M(2+(-1+b)M)+c(2-2bM))^2}{(1+c-bcM+bc^2M)^2})^{3/2}}{8(c+b(-1+c)c)^2},$$

$$c_6 = -\Big(\Big(c^2M^2(-4+12c+3b^3(-1+c)^4c^2M^2+4b(-1+c)(-3+c+3c^2M)+b^2(-1+c)^2cM(-12+3c^2M$$
$$+c(8+M)))\sqrt{4-\frac{(2+(1-2b)bc^3M^2+b^2c^4M^2+bc^2M(2+(-1+b)M)+c(2-2bM))^2}{(1+c-bcM+bc^2M)^2}}\Big)$$

$$\Big/\Big(8(1+b(-1+c))(-1+c)\Big)\Big),$$

$$c_7 = -\Big(\Big(bc^3M^3(8(-2+c+3c^2)+3b^4(-1+c)^5c^3M^3+2b^3(-1+c)^3c^2M^2(-9-2c(-4+M)+3c^2M)$$
$$+b^2(-1+c)^2cM(-36+3c^3M^2-2c(-8+7M)+c^2(12+22M-M^2))+2b(-1+c)(-12+3c^3M(2+M)$$
$$-2c(2+5M)-2c^2(-4-8M+M^2))))\Big/\Big(8(1+b(-1+c))(1+c-bcM+bc^2M)\Big)\Big),$$

$$d_1 = \Big(bc^3M^3(4c^2M+b^4(-1+c)^4c^3(1+c)M^3+2b^3(-1+c)^3c^2M^2(3+3c+c^2M)+b^2(-1+c)^2cM(12$$
$$-2c(-8+M)-c^2(-10+M)M+c^3M^2)+4b(-1+c)(2-c(-4+M)+c^3M^2+c^2(2+M))\Big)$$
$$\Big/\Big(4(1+c-bcM+bc^2M)^2\sqrt{4-\frac{(2+(1-2b)bc^3M^2+b^2c^4M^2+bc^2M(2+(-1+b)M)+c(2-2bM))^2}{(1+c-bcM+bc^2M)^2}}\Big),$$

$$d_2 = \frac{bcM(2+c^2M+bc^3M-c(-2+M+bM))\sqrt{4-\frac{(2+(1-2b)bc^3M^2+b^2c^4M^2+bc^2M(2+(-1+b)M)+c(2-2bM))^2}{(1+c-bcM+bc^2M)^2}}}{4+4b(-1+c)},$$

$$d_3 = -\frac{bc^2M^2(2+bcM(c-1))(2+c^2M+bc^3M-c(-2+M+bM))}{2(1+c-bcM+bc^2M)},$$

$$d_4 = -\Big(\Big(bc^4M^4(2+bcM(c-1))^2(2+c^2M+bc^3M-c(-2+M+bM))(2c+b^2(-1+c)^3cM$$
$$+b(-1+c)(-2+cM+c^2M))\Big)\Big/\Big(8(-1+c)(1+c-bcM+bc^2M)^2$$
$$\times\sqrt{4-\frac{(2+(1-2b)bc^3M^2+b^2c^4M^2+bc^2M(2+(-1+b)M)+c(2-2bM))^2}{(1+c-bcM+bc^2M)^2}}\Big)\Big),$$

$$d_5 = -\Big(\Big(b^2(-1+c)c^3M^3(8-2(-1+b)b^2c^6M^3+b^3c^7M^3+bc^5M^2(b(6-4M)+M)-4c(-4+M+3bM)$$
$$+2c^2(4+b(-2+M)M+3b^2M^2)+2bc^4M(2-3(-1+b)M+(-1+b+b^2)M^2)+c^3M(4-6b^2M$$
$$-b^3M^2+b(12-8M+M^2)))\Big)\Big/\Big(8(1+b(-1+c))(1+c-bcM+bc^2M)\Big)\Big),$$

$$d_6 = \Big(bc^3M^3(2+c^2M+bc^3M-c(-2+M+bM))(-4+12c+3b^3(-1+c)^4c^2M^2+4b(-1+c)(-3+c+3c^2M)$$
$$+b^2(-1+c)^2cM(-12+3c^2M+c(8+M)))\Big)\Big/\Big(8(1+b(-1+c))(-1+c)(1+c-bcM+bc^2M)\Big),$$

$$d_7 = -\Big(\Big(bc^2M^2\Big(-\frac{1}{(1+c-bcM+bc^2M)^2}b(1+b(-1+c))(-1+c)c^2M^2(4+(1-2b)bc^3M^2+b^2c^4M^2$$
$$+bc^2M(4+(-1+b)M)+c(4-4bM))\Big)^{1/2}(3b^3(-1+c)^4c^2(1+c)M^2+2(-2+3c)(2-c(-2+M)+c^2M)$$
$$+2b^2(-1+c)^2cM(-6+c^2(5-2M)+c(-1+M)+3c^3M)+b(-1+c)(-12-4c-4c^3(-4+M)M$$
$$+3c^4M^2+c^2(8-4M+M^2)))\Big)\Big/\Big(8(1+b(-1+c))^2(-1+c)\Big)\Big).$$